# Innovative solutions of air distribution in operating rooms for increasing the degree of thermal comfort and asepsis



# PhD Supervisor:

Assoc. Prof. PhD. Eng. Ilinca Năstase

cotutelle

Assoc. Prof. PhD. Eng. Tiberiu Catalina

PhD Student: Eng. Laurențiu Tăcutu

# **Content:**

| 1  | Intro                             | oduction                                      | 4  |  |  |
|----|-----------------------------------|---|----|--|--|
|    |                                   |   |    |  |  |
|    | 1.1.                              | Overview and objective                        | 4  |  |  |
|    | 1.2.                              | Content and approaches                        | 4  |  |  |
| 2. | . Dyn                             | amic and static situations in Operating Rooms | 5  |  |  |
|    | 2.1.                              | Static situations                             | 5  |  |  |
|    | 2.2.                              | Dynamic situations                            | 5  |  |  |
| 3. | . Expe                            | erimental part                                | 5  |  |  |
|    | 3.1.                              | Equipment                                     | 6  |  |  |
|    | 3.2.                              | Experimental stand                            | 25 |  |  |
| 4. | . Nun                             | nerical part                                  | 33 |  |  |
|    | 4.1.                              | The configuration of the numerical case       | 33 |  |  |
|    | 4.2.                              | Equations and parameters used                 | 35 |  |  |
| 5. | . Resi                            | ults  | 36 |  |  |
| 6. | . Discussions and future studies4 |   |    |  |  |
| Bi | ibliogra                          | phy   | 48 |  |  |
|    |                                   |   |    |  |  |

### Abbreviation:

ASHRAE - American Society of Heating Refrigerating and Air Conditioning Engineers

CCD - charge-coupled device

CMOS - complementary metal-oxide-semiconductor

DIN - Deutsches Institut für Normung

HVAC - Heating, Ventilating and Air Conditioning

ISO - International Organization for Standardization

MRT - Mean Radiant Temperature

OP - Operating Room

PIV - Particle Image Velocimetry

PMV - Predicted Mean Vote

PPD - Predicted Percentage of Dissatisfied

SET - Standard Equivalent Temperature

TE - Equivalent temperature

### Nomenclature:

GT = global temperature [°C]

 $k_c$  = heat transfer coefficient by convection

 $k_r$  = linear heat transfer coefficient by radiation

MRT = radiant average temperature [°C]

OT = operative temperature [°C]

 $T_a = air temperature [°C]$ 

 $\Delta t = time\ interval\ [s]$ 

 $\Delta x = space\ interval\ [mm]$ 

$$v = velocity\left[\frac{m}{s}\right]$$

 $\omega = vorticity$ 

# 1. Introduction

## 1.1. Overview and objective

This PhD thesis aims to clarify and improve some aspects related to the microclimate of the Operating Rooms (ORs) that regards the comfort of the occupants, the aerosols dispersion, the fluid mechanics involved near the operating table. In the first two reports we analyzed the current situation of the clean rooms, focusing on OR, and the actual level of knowledge about them. The first report includes the history of the clean rooms, with emphasis on those from hospitals, a list and details regarding the comfort factors, the comfort indices, the clean room standards and the ventilation methods used for ORs. In general, it includes a review of the literature from scientific articles, books, standards and other technical documents that had a significant importance. In the second report we discussed about the parameters needed to be monitored in the OR, parameters that also help in classifying the ORs as clean rooms, the methods and the equipment's used to measure and determine these parameters, future new approaches that are possible and some preliminary results obtained from some experimental measurements.

The third report contains numeric simulations and experimental measurements made so far. This are related to the thermal plume of the patient and the surgeon and some experimental studies on passive solutions that can improve air distribution in the ORs. The experimental measurements made so far come to validate, through the results obtained, the numerical models made of the OR. This report will also describe the equipment used and the ones that will be used in future studies, the numerical models of the OR, the static and dynamic situations that are found in the ORs and future studies that we want to do in this domain. Thus, future studies will regard the comfort level of the occupants, ways to increase it by passive solutions, the fluid mechanics around the surgical area in a bend position of the doctors over the patient, local ventilation with different type of grilles and there affect.

# 1.2. Content and approaches

This third report includes the numerical studies and the experimental measurements made so far, a wide description of the equipment used and that will be used for future studies, passive solutions to improve air distribution in the OR that have been identified up to this point. Also, this report will contain the numerical models made and how we want to improve them, more details regarding the dynamic situations that can be found in the ORs in order to have an overview of these situations for understanding better the problems and, therefore, for trying to find solutions to them.

The experimental measurements are related to the thermal plume of the patient and the surgeon, the grilles used as passive solutions to improve the ventilation in the OR and comparations between the grilles. The data obtain from the numerical studies and experimental measurements, related to the thermal plume of the patient, are appropriate

and can consist in the first validation of the numerical model. The thermal plume of the patient, surgeon represents an interesting filed because of study because they can have a negative effect on the ventilation system or can be connected to the thermal sensation of the patient or surgeon. It is very well known from the current practice that the patient thermal comfort and of the medical staff has to suffer in the majority of the cases (1, 2). Also, the fact that we didn't find, in the literature, experimental and numerical studies for the thermal plume of a patient suggested us that it can be worthy field to start on. Besides the passive solutions that we thought about, we have taken in to account also some active solutions like the possibility of implementing local ventilation. If this local system will be a plausible solution to implemented, then we will study the effects that this system can have on the thermal comfort and aerosol dispersion.

# 2. Dynamic and static situations in Operating Rooms

#### 2.1. Static situations

When we want to study the microclimate of a room, regardless of its specific, we must make a scenario that includes how the space will be used, the type and number of people, what type of installations are needed, the way that the installations will function and many other things. Obvious, this scenario its related to the specific of the room. When we want to study the problems found in the ORs, you find out that because of the complexity and the high number of parameters that you must take in to account, the majority of the analysis and the studies from the literature are simplified, considering static situations. Also, measurements for validate the clean rooms, according to norms, are made firstly in static situation and some with reference regarding the dynamic situation.

# 2.2. Dynamic situations

The transient state for the ORs takes in to account the different air temperature supply from the air terminals, the movement of the occupants, the movement of the equipment created by the occupants, the frequent opening of the doors or the thermal plume of each occupant.

Some standards bring in discussion the validation of the OR, as a clean room, also when it is in full operation, but they do not give specifics or details, just mentions. Thus, this brings a lot of misunderstandings. This misinformation's are because of the complex phenomena that need to be taken into account that also depends on the specifics of each OR.

# 3. Experimental part

The OR has an essential role in today's society and because of this aspect the study of their microclimate and of the involved fluid mechanics is very important. Given the technological development in the last century, this allowed a more profounder study of this field with far more advanced means. Due to these aspects, some have studied the microclimate in the OR from experimental and numerical perspectives (3-5). In our days, the experimental studies can consist in real-scale ORs, dedicated measurement equipment for temperature, humidity, velocity, aerosols or thermal comfort and specific measurement technology like thermal manikins, particle image velocimetry (PIV), laser doppler anemometry (LDA) and others. Compared to classical measurement systems which give the possibility of estimating the global PMV, the thermal manikin gives the advantage of assessing locally a predicted sensation, either through the equivalent temperature or either through a derived local PMV. In other words, the thermal manikin is a method of investigating the local discomfort trough the local distributions of the equivalent temperature on the segments of the manikin. Also, the thermal manikins with anatomical shape can be used measurements that are harmful to humans, like PIV measurements, and keeping the accuracy of the measurements like using a real person. Thus, the thermal manikin represents a worthy tool for the thermal comfort analysis in laboratory configurations and in real field case studies. This kind of representation allows for instance, the inspection of the uniformity of an environment. The thermal manikin also allows the possibility of experimentally validated numerical models by measuring its thermal plume and investigating its interaction with the global environment.

## 3.1. Equipment

#### Thermal manikins

A very useful tool in today's research in the field of microclimate and thermal comfort for indoor environment represents the thermal manikins. Thermal manikins can simulate the temperature of a human subject or, for the most advanced manikins, they can simulate even the sweating or the breathing. In this case, they can simulate the heat transfer between the manikin and the ambient, stimulating the body's thermoregulatory system, and also the mass transfer. The first thermal manikin related in history was the model made by Gagge A.P. (6-9) used for studying the interaction between the manikin and the indoor environment. The first manikin made by Gagge had a heat source to simulate the metabolic rate, the motion (mechanical work) of the muscles, and a membrane with the role of simulating the skin, in order to study the heat flux from her. Since then, they have been used continuously in military applications regarding the heat transfer through clothes or civilian applications regarding the indoor environment, ventilation strategies, and so on. The purpose of thermal manikin used for indoor environment is to determine the thermal comfort that a human subject would feel in an enclosure. It can be any type of enclosure in which a human subject can carry out his activity, namely a normal enclosure (living room, study room), a transition room (a vehicle), special premises (OR). The thermal comfort can be considered local, a local discomfort like a draft sensation, or a global one, like PMV and PPD. This can be done due to the possibility of determining the instant temperature of the surface of the manikin and the equivalent temperature that is calculated in accordance with

the thermal comfort standards. The temperature of the segments of the manikin will be set according to the average temperatures found on the respective segment of a human subject. Also, for calibrating the manikin a certain temperature is required. All these temperatures are found in the literature, either norms or specialized technical books. The thermal manikins have evolved from geometries with parallelepipedal segments to humanoid shapes. The humanoid thermal manikin it's also helpful in measurements that need to study the human body but are harmful to humans, like Particle Image Velocimetry (PIV) measurements.



Fig. 1 – Thermal Boy in the surgeon position

For the studying of thermal comfort, we use two humanoid shape thermal manikins. The first humanoid thermal manikin developed is called "Thermal Boy", a male model (figure 1). This thermal manikin has a vertical posture, with a height of ≈1.73 meters and a surface area of ≈1.8 m². He is made of a plastic humanoid manikin on which is mounted electric circuits and sensors. The current passes through the electric circuits and heats up the heating elements that we called them patches. These patches are made out of fin silicone (1.5mm) which have a nickel wire and a protective foil. The circuits are supplied by a DC source at 24V. The heating power of a patch is 24W. These patches were glued with a double-sided tape, being careful to follow the shape of the manikin as faithful as possible.

Thermal Boy has 39 patches that are grouped in segments and each segment represents an anatomical component. Also, in the literature the segments can be found under the name of regions or zones, but they represent the same thing. Each segment (region or zone) represents a part of the human body like the head, right or left hand, core, right or left leg. Each patch is controlled independently. Thermal Boy also has the possibility to be coupled with a breathing circuit.

As a general working principle of the thermal manikin, the patches are injected with electric current (DC) from the electric source, the sensors continuously transmit information to the acquisition board regarding the surface temperature and when the temperature reaches the set point, the electric current injected stops gradually with the help of the microcontroller.

The patches were designed to cover exactly each area of the manikin. For this manikin there were selected 5 types of patches, in order to cover the entire surface and keeping the costs low. Each patch has 4 transducers that are controlled by a microcontroller. The temperature shown for a patch represents the median temperature of all 4 sensors.

Thermal Boy has its own acquisition board (figure 2) and the software is "in-house made" (figure 3). Because of the density of the electric circuits that are near the acquisition board and the core, when the manikin is measuring over a long period of time, the heat released from this high density of electric circuits is very high and tends to increase the temperatures in that zone. Because of this, the operator must be careful and check the temperature in the zones with high density of electric circuits when its measuring over a long period of time. The temperature can be check by monitoring each zone and with external equipment's like a IR camera.

The software allows to control, read and record the surface temperature of each patch.



Fig. 2 – A mounted patch (24V, 24W) and the acquisition boards of Thermal Boy

In the main graphical interface of Thermal Boy (figure 3) we can see if the software has connected to the PC, we can load the setpoints (temperatures) for each patch and we can see the temperature of the patch or segment and the power injected. Also, the software gives the possibility to hide a patch or segment temperature and power, thus not injecting current in it. The temperature data is saved in a txt file with all the data selected.



Fig. 3 – Graphical interface of Thermal Boy, power and temperature of every patch

A basic scheme of how Thermal Boy functions is shown in figure 4. Here we can see, in general terms, the flow data and key components for this system.

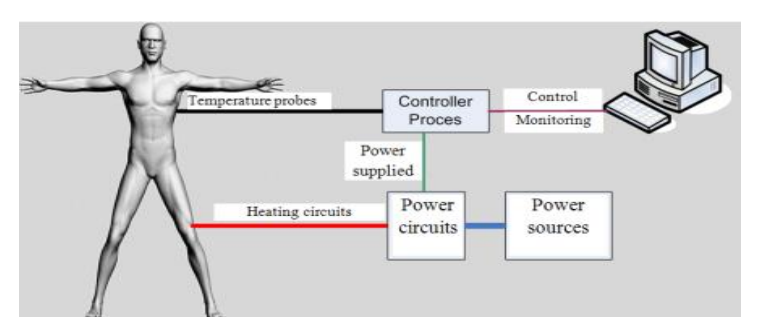


Fig. 4 – A simplified operating scheme of Thermal Boy

The second humanoid thermal manikin and the most advanced is called "Suzy". Suzy is made from a plastic medical manikin, a female model, that has a very good degree of flexibility and a height of ≈1.66 meters with a surface area of ≈1.60 m². She has 79 patches that are grouped in segments, each segment represents an anatomical component. The patches are mounted so that they can give the humanoid form as faithful as possible. Each patch has 5 transducers controlled independently by a microcontroller. She has, in total, 395 transducers. The temperature shown for a patch represents the median temperature of all 5 sensors. The patches were attached in the same way as for Thermal Boy. The zones with the patches are represented in figure 5. Here we can see the front and back view. The black dots represent the joints and the red patches represents the lateral zones.

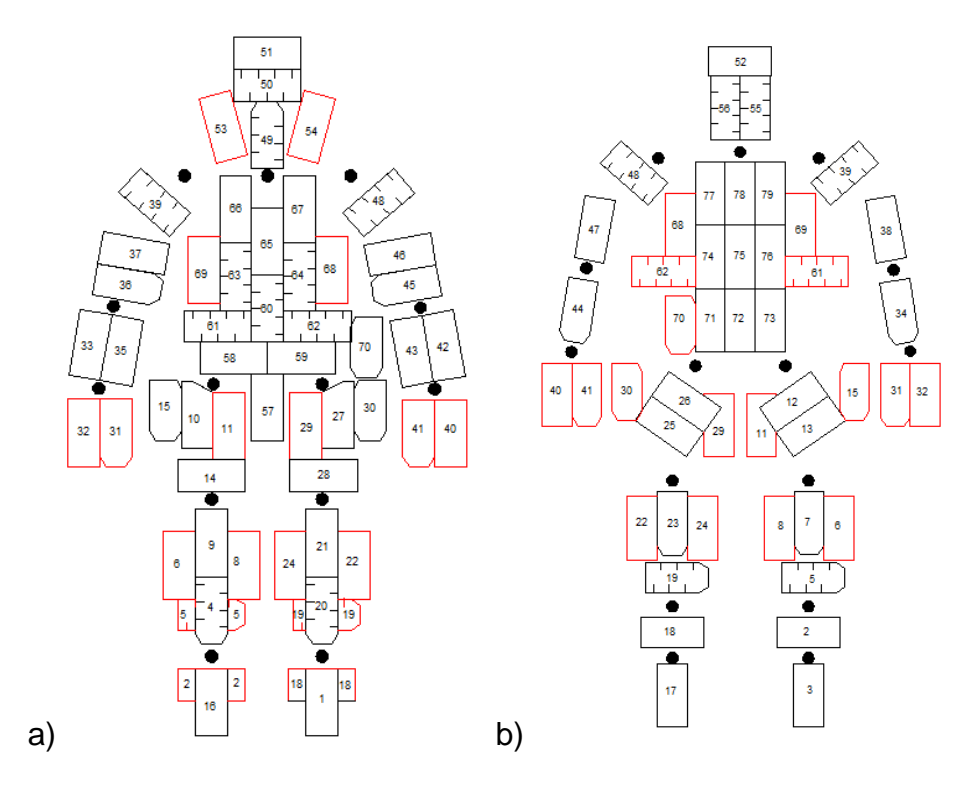


Fig. 5 - Paces placement: a) Front view; b) Back view

The software for this thermal manikin was made in the visual programming language called LabVIEW. This manikin its controlled by a neuro-fuzzy controller.



Fig. 6 – Suzy in the patient position

Suzy and Thermal Boy have two predefine setpoints, one with 34°C temperature on each segment and another similar with the human body temperatures for each segment. The first temperature setpoint (34°C) is used initial for calibrating the manikins. Besides these two predefined options, we can make our own setpoints if the measurement that we will make will required this.

In the figures 7 and 8 we can see better the graphical interface of Suzy, which is made up of three interfaces. In the first interface (figure 7) we can set the temperature of each region, the measurement time (shown as 300s) and the option to exclude the overheat patches. Figure 7 has in the left part of the picture the setpoints for each segment, with the temperature setpoint corresponding to a human body, and in the right side three graphics with the mean temperatures for each patch, the power absorbed for each patch and segment. Thus, in the left of the picture, in the upper part, we can see the segments and in the lower part we see the number of patches that each segment has. Also, here we can see better that each patch can have a different temperature as setpoint. In the right side of the picture we can see a graphic with mean temperatures for each patch and the power absorbed for each patch and for each segment. Here we have the option to hide, in the graphical display or for measurement reading, patches or segments. The measurement time that is set here to 300s can be change but the measuring will begin when the start button will be pressed. Another option that can be accessed here is the one to remove from overall power averages those certain patches that are close to the controller and acquisition board and then to heat up because of the high density of electronics near them. Thus, they tend to heat up and consume less power. Activating this controller can be done by pressing the button "exclude overheat patches".

In another interface (figure 8) the user can see in the right side a humanoid map of the manikin on which we can read instant temperatures or equivalent temperatures.

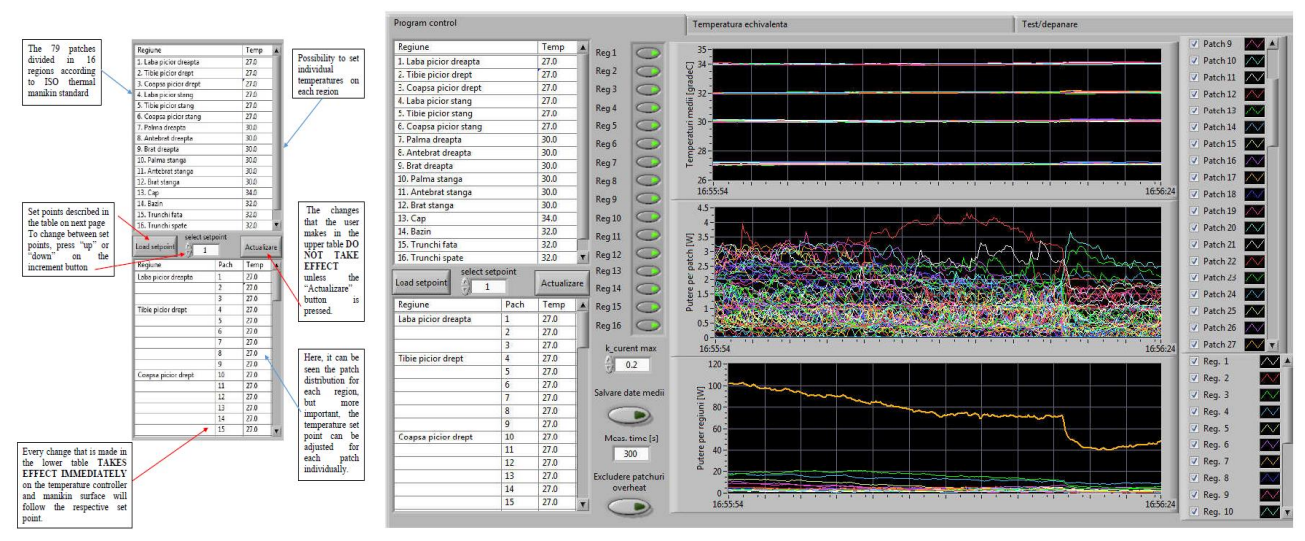


Fig. 7 – Suzy command panel with graphical interface: left – temperature and power per region, right – equivalent temperature per region

In this interface we must change the coefficient to the setpoint selected in the first inferface (different temperature or 34°C) in order to have a correct temperature display on the humanoid map. In the left side (figure 7) it's shown the temperature and the power absorbed for each segment, while in the bottom we have the option to change between setpoints and to change the length of the sliding average required for the equivalent temperature calculation (in seconds).

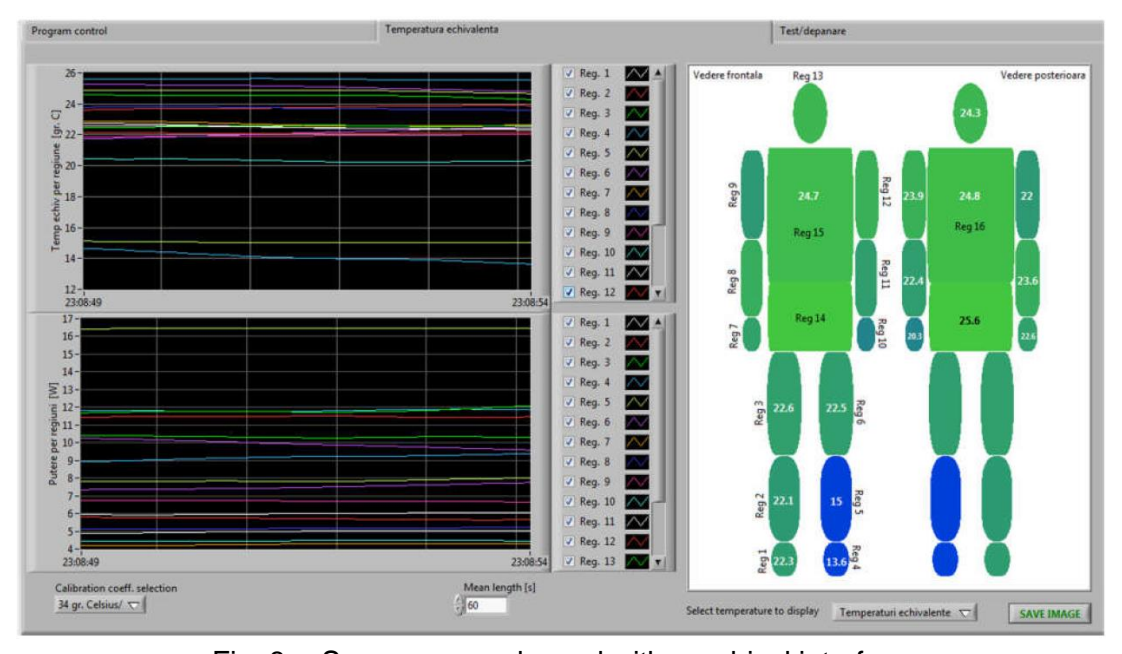


Fig. 8 – Suzy command panel with graphical interface: left – temperature and power per region, right – equivalent temperature per region

The equivalent temperature formula is expressed mathematically as the difference between the temperature per that region, that is a mean of all the sensors in the patch, and the report between the power injected in the patch and the product of that surface and a convective heat transfer coefficient:

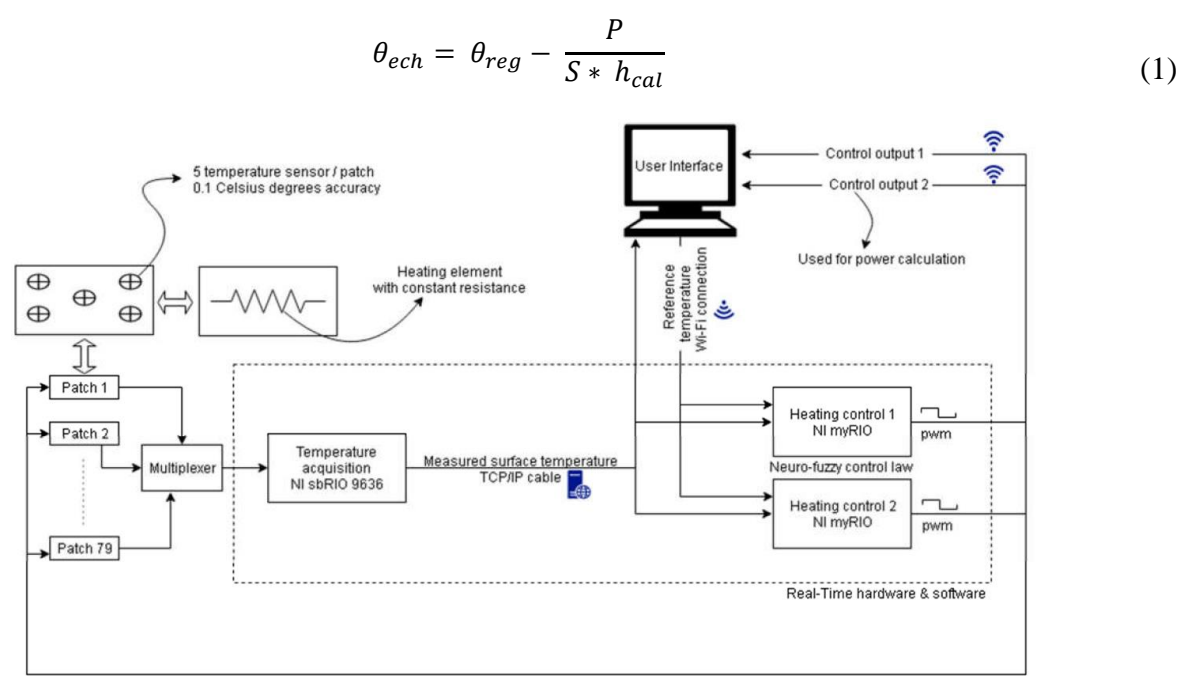


Fig. 9 – Suzy thermostatic system

The system was designed to address future problems, to help with troubleshooting by making an option to detect faulty transducers.

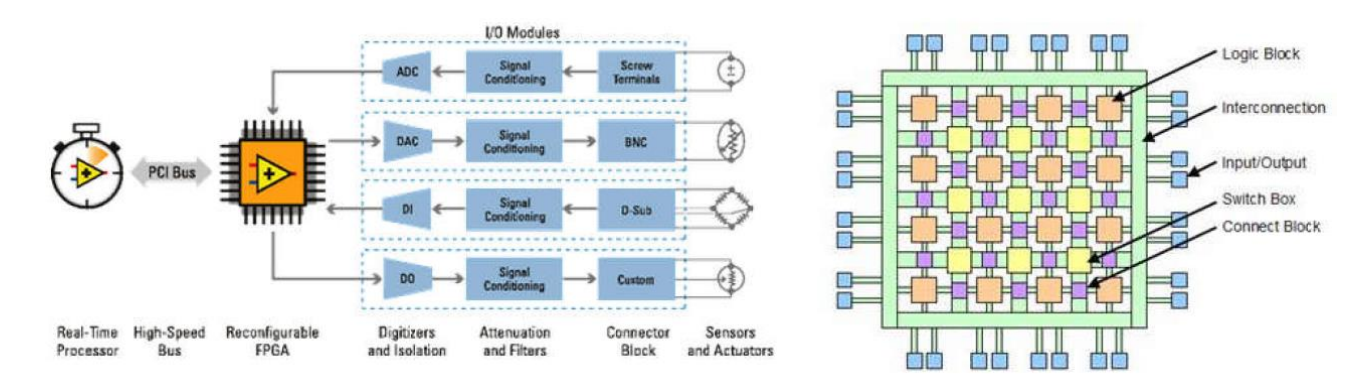


Fig. 10 – National Instruments (NI) typical architecture (left) that is based on a field programmable gate array (FPGA) (right)

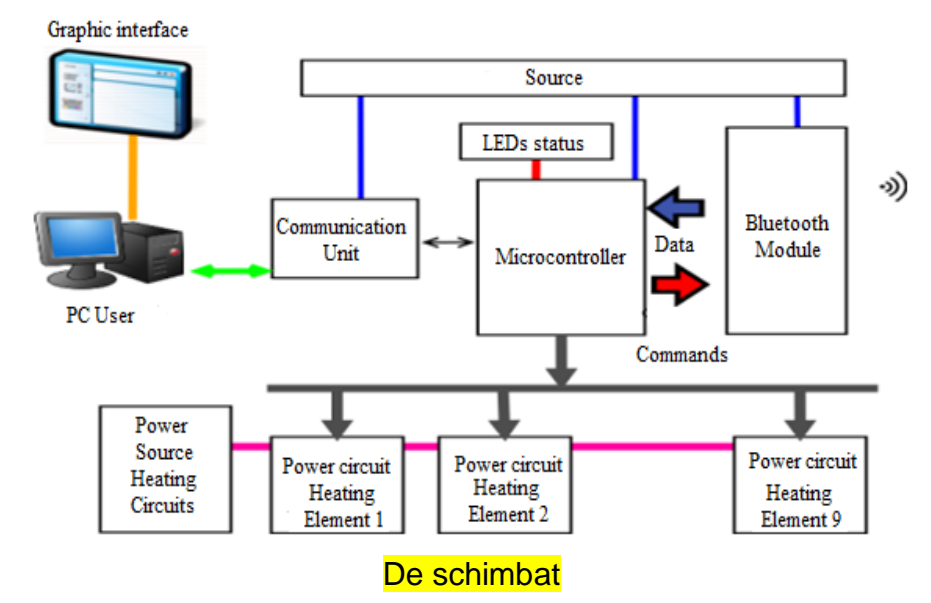


Fig. 11 – A simplified operating scheme of Suzy

The main power supply for heating the patches can be seen in figure 14, a, the power supply used for myRIO boards (temperature controller) can be seen in figure 14, b and the the power supply used for the sbRIO boards (temperature acquisition) is shown in figure 14, c.



Fig. 12 – Power sources for: a) patches; b) temperature controller; c) temperature acquisition

Suzy has also the possibility to be coupled with a breathing circuit. Thus, she will be improved by adding a respiratory system in order to stimulate the respiratory circuit of a

human body. The respiratory system represents an external equipment which has, among many other components like electronic and hydraulic components, a main unit that consists in a piston compressor. This system and his components can be seen in figure 13. For implementing this breathing circuit to Suzy or Thermal Boy a dedicated software language must be made and correlate with the ones used for the manikins.

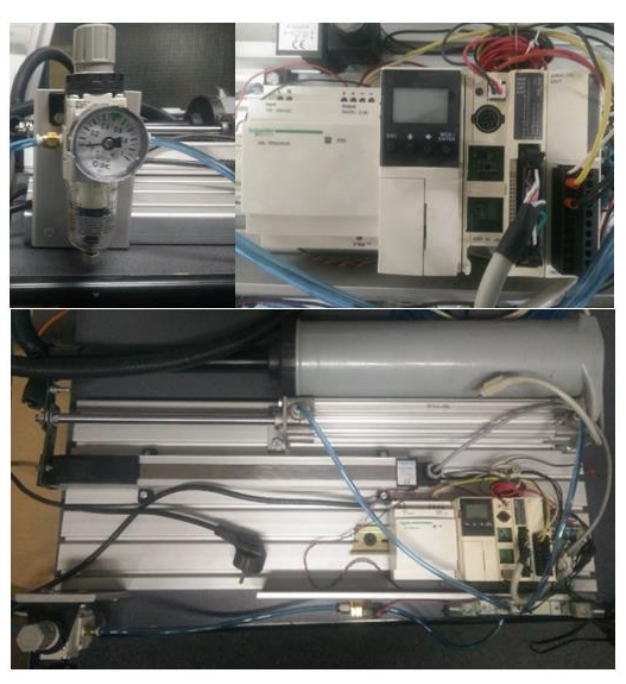


Fig. 13 – The breathing circuit thought initially

Another tool that we use for making indoor comfort measurements is ComfortSense. This system is designed for research or measurements in HVAC systems that requires multipoint measurements for air temperature, velocity and humidity. ComfortSense is a measurement system developed by Dantec Dynamics that determines the comfort in accordance with the following standards EN 13182, ISO 7726, ISO 7730, ASHRAE 55 and 113. The system can make measurements of air speed, temperature, operating temperature, determining the PMV, PPD indices and also draft sensation. In general, the system consists in a main unit that can have up to 16 inputs for measuring probes and different types of probes that measures the parameters mentioned above. The main unit processes and transmits the information to a personal computer (PC) to read and save the data. Thus, it has built-in A/D (analogical/digital) converter with a USB 2.0 interface, microprocessors and other microelectronic components that are required to perform the operations. Also, for cases where there is no possibility to connect the unit to an electricity network the manufacturer offers the possibility of a power battery. The main unit with the input modules and the battery can be seen in figure 14.







Fig. 14 – Dantec a) Central unit; b) Input module and assembly; c) Power battery (10)

The probes used measure parameters like air temperature, speed or humidity. This are needed to calculate the draught sensation, the PMV and PPD indices or the operative temperature. For draught measurements an omnidirectional sensor is required that has a frequency response of at least 2Hz. The omnidirectional probes used in this system measures both air velocity and temperature. The probe used for measuring the draught is made of a thin film, for measuring the velocity and a small thermistor with fast response, which measures the temperature.

The velocity sensor consists of two quartz spheres of 3 mm diameter, wrapped with a thin nickel sheet that is covered with a layer of quartz. As a measurement principle, one of the spheres is maintained at a higher temperature than the other while the electrical energy required to maintain it at that higher temperature is measured. A special algorithm makes the conversion between the measured temperature, heat loss, convection coefficients, air velocity. These two spheres are protected by a cage to prevent mechanical damage. Due to the simple and thin construction, obstruction of the air flow is minimal. The probes can be mounted on tripods or crossing beams systems, which can be static or dynamic during measurements. ComfortSens has also compact flexible probes, designed to be placed on manikins, for determining the draught sensation (picture 15). The speed and temperature probe can measure velocity with between 0.1÷30 m/s and temperatures between -20÷80°C.

The humidity probe measures humidity based on the hygroscopic properties of a polymer that is contained between two electrodes. The thin polymer sheet absorbs or releases water vapor, depending on the relative humidity of the room. The dielectric properties of the thin sheet of polymer depends on the amount of water vapor that is stored in it. Therefore, depending on how the relative humidity changes, the dielectric properties of the sheet change and thus the capacity of the sensor changes.

The operative temperature probe has an ellipsoidal shape, with a diameter of 56 mm and a length of 160 mm. The sensor element is a nickel wire coil which measures the average temperature on the ellipsoidal surface. The shape and size of the sensor facilitates the direct measurement of the operative temperature, its shape being chosen because different surfaces, that are cooler or warmer, may have similar effects on the sensor as it would have on the human body. The sensor can simulate a person standing when he is positioned vertically, a person seated when it is bent at a 30° angle to the vertical, and a person lying down when positioned horizontally. The measuring element has the surface

color and structure as close as possible to an average-dressed person with normal clothing.



Fig. 15 - ComfortSense probes

A dedicated application software is provided by the manufactured to read and make a graphical presentation with the data received by the probes. The results can be made in a 2D and 3D graphic. The software includes a library with probes in order to be easily identified and used. After selecting the probes, the software allows their placement in space and a route if they do not have a fixed position. The temperature and humidity range are defined by the user and the program notifies the user when these values are exceeded. The software performs parameter linearization, statistical calculations and spreadsheet or graphical presentations. It can export the results as text or for programs like Office Excel (figure 16).

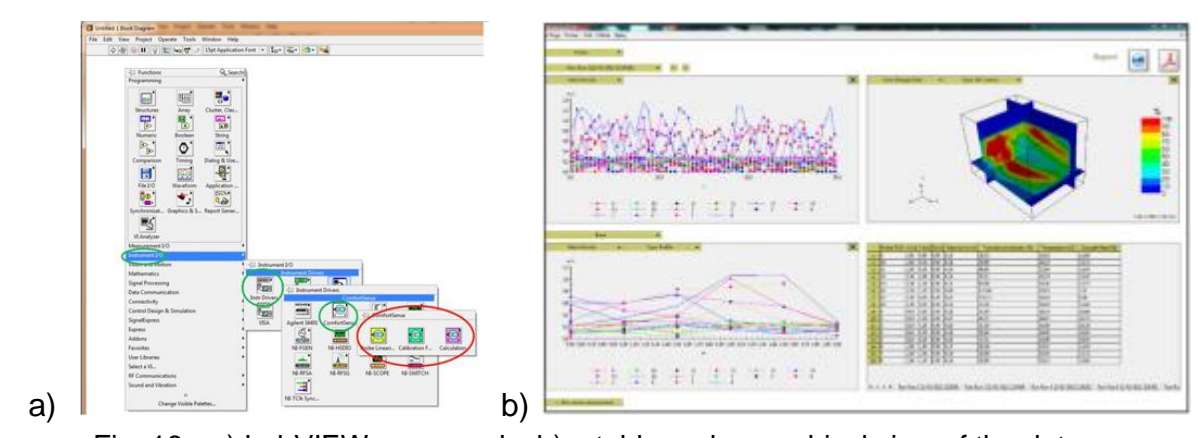


Fig. 16-a) LabVIEW commands; b) a table and a graphical view of the data

A brief review of what each parameter mentioned above, that ComfortSense can determine, will be made further. Operating temperature (OT) is defined by ASHRAE standard as "the uniform temperature of an imaginary black enclosure, where the occupant changes the same heat transfer through convection and radiation, similar to a non-uniform enclosure".

Mathematically, it is expressed as a weighted average of MRT and Ta with the respective transfer coefficients:

$$OT = \frac{k_r MRT + k_c T_a}{k_r + k_c} \tag{2}$$

Operational temperature integrates the effect of air temperature and radiation effect, but ignores the effect of humidity and air movement. Corrections were made to this index in order to attempt to integrate the effect of humidity and air velocities, but corrections for air velocity are generally not acceptable. ASHRAE (11) states that for occupants who are employed in near sedentary activities (with a metabolic rate between 1.0÷1.3 met), in conjunction with no direct effects of solar radiation and air velocities greater than 0.20 m/s, it is acceptable that the OT relationship to be write as:

$$OT = \frac{T_a + MRT}{2} \tag{3}$$

The most widely known and accepted methods for determining thermal comfort are Fanger's equations (12), namely its "Predicted Mean Vote (PMV)" and "Predicted Percentage of Dissatisfied (PPD)" (13).

Thanks to these methods, a series of standard and technical documents were produced, such as Fanger 1980, ASHRAE 1981, ISO 1984, Jokl 1987 (7). Hensen (14) states that only ASHRAE 1981 mentions acceptable limits for dynamic situations and that, conventionally, thermal discomfort is treated as a subjective condition and thermal sensation as an objective condition. Due to the multitudes of variables and unknowns, which make the thermal comfort a complex topic, they point to the fact that there is not an absolute standard for thermal comfort (15).

There are currently two approaches to study the thermal comfort, the rational approach or heat-balance and the adaptive approach (15). The rational approach or heat-balance is based on the study made by Fanger (16).

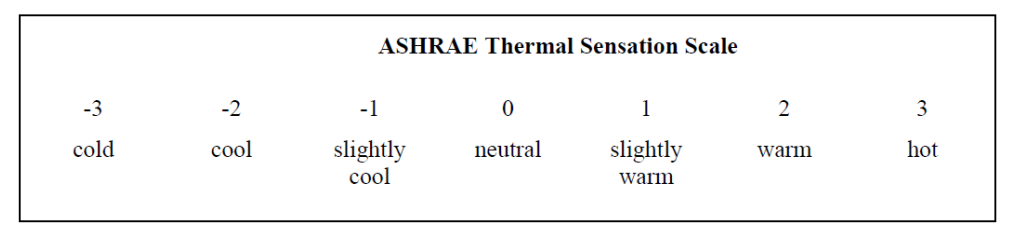


Fig. 17 – ASHRAE thermal comfort rating scale (PMV) (17)

The mathematical expression of the PMV index between the thermal flux released by the human body in an environment and the temperature required for optimum comfort when carrying out a particular type of activity is:

$$PMV = [0.303 \exp(-0.036M) + 0.028]L = \alpha L \tag{4}$$

Where M is the metabolic rate of the organism, L is the thermal load on the human body, defined as the difference between the heat produced by the body and the heat delivered to the environment, and  $\alpha$  is the sensitivity coefficient.

The PMV index can predict the average thermal sensation for a group of people, but it should be kept in mind that in this group the optimal thermal conditions may vary from one individual to another by about 1.15 ° C or even a unit as ASHRAE scale. Besides this index, Fanger has developed an index that can estimate the percentage of dissatisfied people (PPD). This PPD is the result of PMV, and both can be expressed in a graphical form U (figure 18).

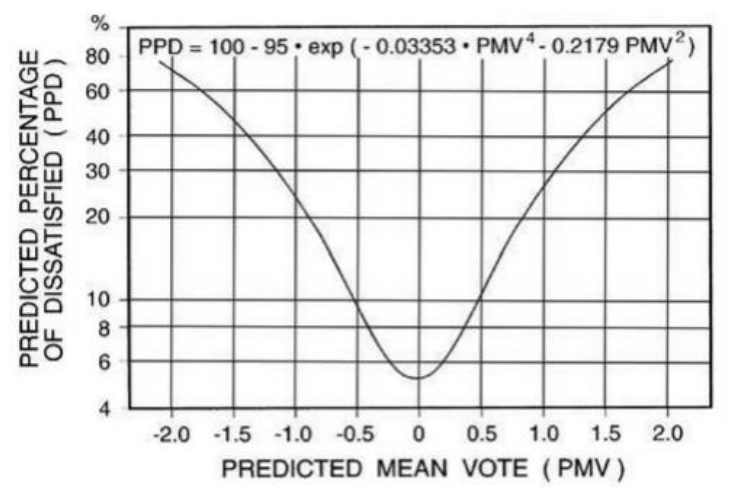


Fig. 18 – PPD as a function of PMV (18)

The relationship between PMV and PPD is:

$$PPD = 100 - 95 \exp\left[-(0.03353PMV^4 + 0.2179PMV^2)\right]$$
 (5)

A first interesting observation, also mentioned by Fanger, from the PMV-PPD graph (figure 18) is that even if a neutral thermal comfort condition is created, according to PMV index and of thermal comfort rating scale, there would still be a percentage of people, around 5%, who would feel a discomfort, too hot or too cold. ASHRAE has made a table listing all six variables that account for the PMV index. These are shown in Table 1, which specifies the four physical variables (air temperature and speed, mean radiant temperature, relative humidity) and the two personal variables (clothing degrade and activity level).

| ruble i Mornica definition conditions (15) |                                     |  |   |  |
|--|-------------------------------------|--|---|--|
| Season                                     | Optimum<br>Temperature <sup>a</sup> | Acceptable Temperature<br>Range <sup>a</sup> | Assumptions for other PMV inputs <sup>b</sup>   |  |
| winter                                     | 22°C                                | 20-23°C                                      | relative humidity: 50% mean relative velocity: < 0.15 m/s mean radiant temperature: equal to air temperature metabolic rate: 1.2 met clothing insulation: 0.9 clo |  |
| summer                                     | 24.5°C                              | 23-26°C                                      | relative humidity: 50% mean relative velocity: < 0.15 m/s mean radiant temperature: equal to air temperature metabolic rate: 1.2 met clothing insulation: 0.5 clo |  |

Table 1 - ASHRAE thermal comfort conditions (19)

It is noted that Table 1 specifies both an optimal temperature and a temperature range in order to achieve the thermal comfort conditions for the percentage of unsatisfied personnel, according to the methods made by Fanger.

Particle Image Velocimetry (PIV) represents a non-intrusive laser optical measurement technique used in research or diagnostics in the field of fluid mechanics, like analyzing the flow, the turbulence, the combustion process or spray atomization and microfluidics. A standard PIV measurement represents a 2D view of the laser plane with the fluid flow seeded, capturing the 2 velocities components (y and x). The capturing represents taking pictures with a charge-coupled device (CCD) or complementary metal-oxidesemiconductor (CMOS) camera. A standard PIV measurement is also abbreviated as 2D2C, representing a 2D view with two components. Also, there are measurements with 2D view but capturing all the three velocity vectors. The abbreviation for this measurement is 2D3C. This measurement is realized using two cameras, also called a stereoscopic (or stereo) PIV measurement. Another type of measurement with the PIV system is volumetric velocimetry which includes making 3D view of the flow and determining all the three components, resulting in a 3D3C abbreviation. The volumetric velocimetry is also called TOPO PIV. For this type of measuring is needed two or more cameras, but most of the time four cameras. Thus, the PIV is a non-intrusive measurement, with planar of volumetric technique, being able to measure flows with velocity range from zero (0) to supersonic, capable of determining two (2) or three (3) velocity components simultaneously, with the possibility to measure areas less than 1 mm<sup>2</sup> and bigger than 1m<sup>2</sup>. The measurement principle its shown, step by step, in figure 19 a) and a slight simplified scheme applied to the flow of a duct is show in figure 19 b). The double-pulsed laser is fires two laser beams at a time interval distance, the beams travels through a two lens, one cylindrical and one spherical, making the light sheet on the target area. The target area represents the flow of fluid that is seeded with particles. A high-speed CCD or CMOS camera is placed perpendicular to the target area, capturing the measurement volume, resulting in two image frames from each pulse (pulse 1 and 2).

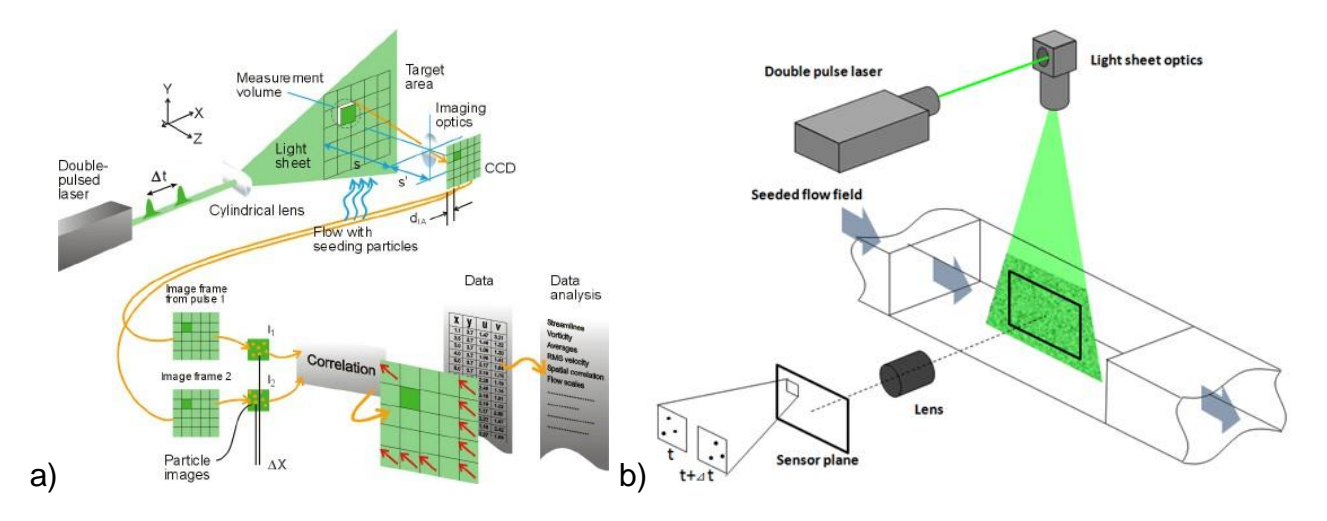


Fig. 19 – PIV system: a) measurement principle; b) simplified measurement principle for a duct (20)

A correlation between the density of the seeding, the velocity of the flow and the time interval between the laser beams must be made in order to make a proper capture of the displacement of the particles. Thus, the operator can set the time interval between the laser beams from the software and, in most of the cases, he can adjust the seeding density and the velocity of the flow. A correlation of the pictures is made by the software, the data can be viewed numerical or graphical. The movement of the particles in time is expressed by the velocity vector in a simple mathematical report:

$$v = \frac{\Delta \bar{x}}{\Delta t} \tag{6}$$

The camera captures each pulse light in an image, resulting in two image frames from the two light pulses. After capturing each pulse light in an image, the images are divided in small subsections called interrogation areas (IA) with the objective to cross-corelate each IA from each frame, I1 and I2, pixel by pixel. For having a good signal peak in the cross-correlation a number of 10 to 25 particles must be captured in each IA. Overlapping two succession IA images will give the displacement of the particles and a visual sense of the flow structure. After the correlation process its obtained a signal peak that is due to the identification of the particle displacement (dx). A subpixel interpolation is applied after in order to make an accurate measurement of the displacement of particles, resulting of course in calculating the velocity. Thus, after this post process we have a vector output. The two IA, I1 and I2, with a displacement of dx and a signal peak are shown in figure 20.

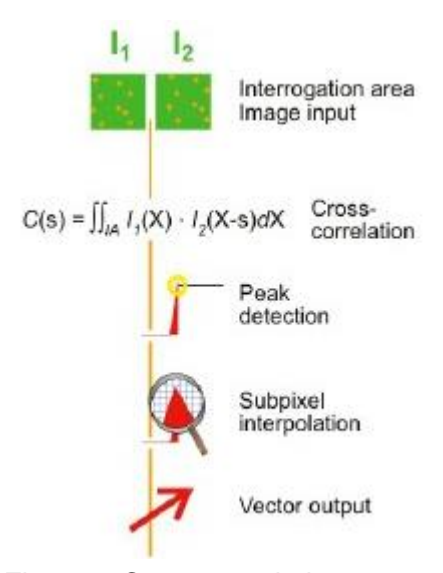


Fig. 20 – Cross-correlation process

In flows that air is the fluid of study, the seeding particles used in general are oil drops from 1µm to 5µm. When studying water flows, the seeding particles is typically polystyrene, polyamide or hollow glass spheres from 5µm to 100µm.



Fig. 21 - Double-pulsed particle images

For defining the measurement volume, we must know the size of the IA, the magnification of the imaging and the light-sheet thickness. Expressing this in a mathematical equation we get the side length of the interrogation area (dIA) and the image magnification (s`/s), with a velocity gradient small in the IA:

$$\frac{\frac{S}{S}|v_{max} - v_{min}|_{lA} \Delta t}{d_{lA}} < 5\% \tag{7}$$

From equation 6 we see that for having a correlation between two images, which means not losing particles that can travel further than the size of IA, in that time interval ( $\Delta t$ ), the highest measurable velocity is constrained. For having not losing the correlation between the two images is enough to respect this proportion:

$$\frac{\underline{s}}{\underline{s}} v \Delta t \over d_{IA} < 25\% \tag{8}$$

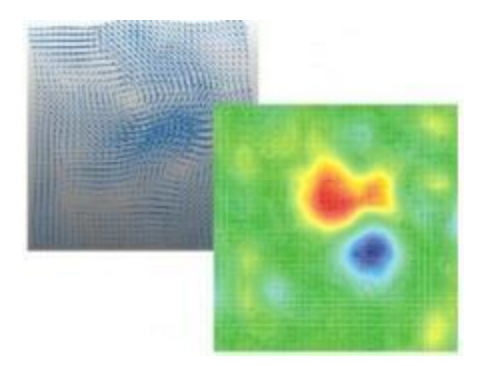


Fig. 22 – A vector map (up left) and a derived vorticity,  $\omega$  (down right)

$$\omega = \frac{\partial v}{\partial x} - \frac{\partial u}{\partial y} \tag{9}$$

For seeing the third component of the velocity vector we must use a stereoscopic arrangement, which means using two cameras for capturing images. An experimental setup for a stereoscopic PIV measurement we can see in figure 23. Here we see in principle how the flow behind the car model is studied with the cameras placed in a diagonal position towards the vehicle. This measurement method is based on the principle of parallax, how we can see in figure 23. The parallax effect represents the difference in the apparent position of an object that is viewed by different observers from two different viewpoints along two different lines of sight, having the observers align on the same axis, and determining the angles between the lines of sight. Applying the parallax effect to picture 23, the object represents the car, the observers represents the cameras, the alignment is on "x" axis and the lines of sight represents the lines of viewing the car. Thus, by placing the cameras so that they observe the light-sheet plane from two different angles, obtaining slightly different two-velocity component vector maps from each camera, we will see difference on the same image captured in the same time, difference resulting from the third velocity component as a cause of the geometrical configuration.

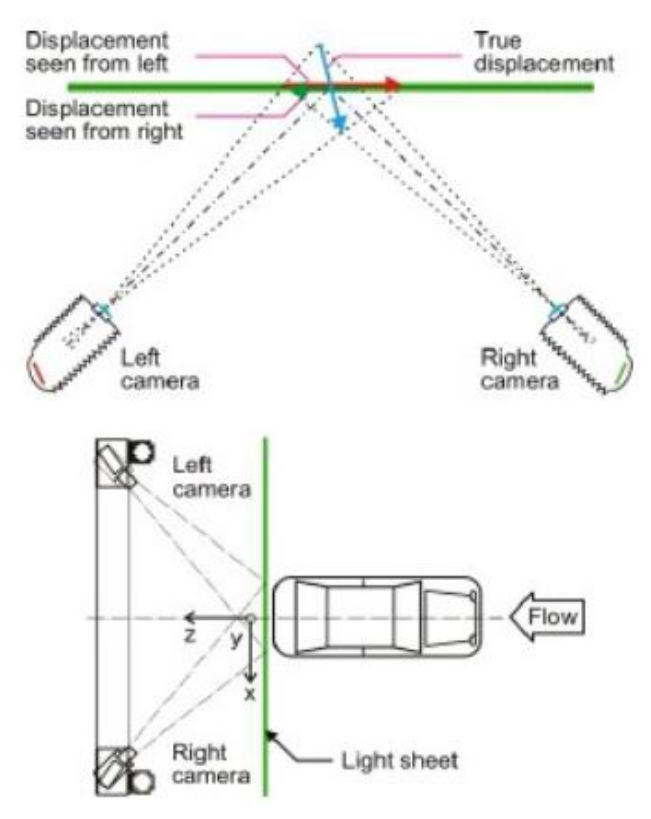


Fig. 23 – Stereoscopic PIV measurement for a car (20)

Also, for correcting the parallax errors, the two velocity components can be recalculated. For capturing in 3D a flow, including the three velocity components, volumetric velocimetry or TOMO PIV is used. This includes more cameras and a more laborious setup with more difficulties in calibration.

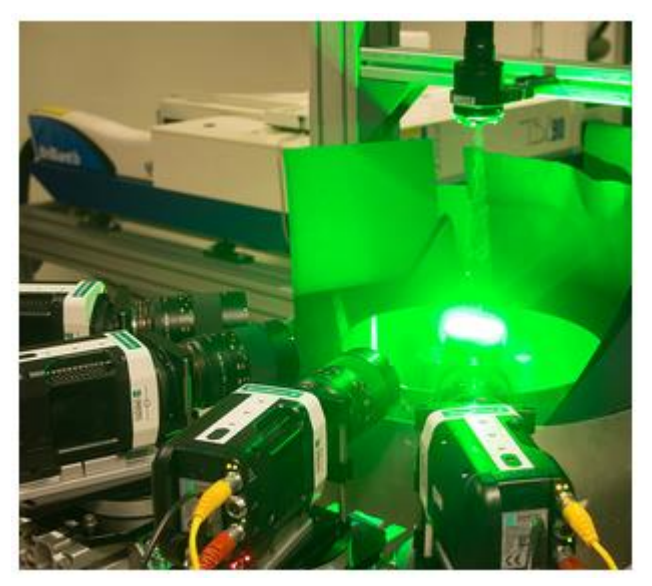


Fig. 24 – Volumetric velocimetry (TOMO PIV) setup for a low swirl burner (20)

In general, configurating the hardware for any measurement tends to be as easy as possible with devices type plug-and-play or software that tries to auto detect the device and load the needed settings. For cable connection there are diagrams and predefined device libraries for knowing how to make the right connections. Also, some automated features are integrated in the software, allowing to control the frame rate, the laser pulse separation or the traversing position for making automat measurements. Of course, for this type of measurements the other equipment's, like cameras, are synchronized with the selected settings.



Fig. 25 – Diagram for connecting the synchronization cables

Other equipment's used in the measurement campaigns were a balometer from TSI, a sound meter from Bruel & Kjaer and a differential pressure gauge from Testo (figure 26). Also, thermocouples were used to determine the temperature of the air or of different surfaces. When working in the field of clean rooms, it is often necessary to measure pressures in related enclosures to measure the rooms pressure for calibrating the HVAC

system and this is done by means of differential pressure gauges. The modern differential pressure gauges are digital, portable, with two tubes mounted on the equipment, each being placed in a enclosure. This equipment helps us determine the static pressure in the different enclosures. Another example of frequent use of this equipment is the measurement of pressure drops on filters from air treatment plants or plenums.



Fig. 26– a) Testo differential pressure gauge for filter pressure loss; b) TSI balometer type ALNOR; c) Bruel & Kjaer sound meter

The balometer is a measurement equipment used to determine velocity and flow. Is made out from a textile cone and measuring equipment which has velocity sensors and the electronics needed for processing. Determining the velocity and knowing the cone section surface at end, it can calculate the flow of the air. This equipment is used to determine the flow of air at the terminal units of a ventilation system. For this reason, it is easy to handle, generally of small sizes, with gaskets that are compressible for a better sealing.

The measurement campaigns were performed in a climatic chamber that has the dimensions of 3.5m x 3.5m x 2.5m (I x L x H). The test cell has active walls and an air distribution system allowing several ventilation strategies to be tested. The air ventilation system was thought to have the possibility of changing the inlets and outlets of the air by closing a damper or making a by-pass.



Fig. 27 – The climatic chamber and his ventilation system

# 3.2. Experimental stand

The experimental stand was organized in the climatic chamber (3.5m x 3.5m x 2.5m, I x L x H) of the Thermohydraulic department from the Faculty of Building Services. The measurements were to determine the thermal plume of the patient and to characterize, from a technical point of view, the passive solutions that consist in eight (8) types of grilles with different geometries. For determining the thermal plume of the patient, we used a PIV system in order to study the flow around the thermal manikin used as a patient. This study was performed in isothermal conditions (20°C). The temperature inside the cell was measured with PT100 temperature sensors which were connected to a data acquisition device. The probes were calibrated for a temperature interval from 0°C to 32°C, with a precision of 0.2°C. On each wall a sensor was placed while six sensors were placed near Suzy's head, on vertical, to have a gradient temperature. PIV measurements and an infrared (IR) camera were used for capturing the thermal plume of the surgeon manikin. The employed IR camera, FLIR B620, has a high-resolution pixel detector of 640x480 pixels, with 0.04 K sensitivity. The employed PIV system was composed of one high sensitivity Flow Sense 4M camera of 4 x 106 pixels resolution and of a Dual Power 200 mJ laser having the wave length of 532nm. The acquisition frequency of the PIV system was 7.5 Hz. The air flow was seeded with a fog generator that uses olive oil. The images calibration gave a spatial resolution of 600 µm per pixel which is corresponding to a 300x300 mm<sup>2</sup> field of view. The number of image were between 300 and 500. The images were processed through an adaptive multi grid correlation algorithm handling the window distortion and the sub-pixel window displacement. The time interval between the shooting of the two laser beams were 1000µs, 1200µs and 1500µs (figure 29). To avoid the presence of reflections we placed black duct tape on the surfaces which intersected the laser plane. This is way of good surface of Suzy's head is covered with black duct tape (figure 28).

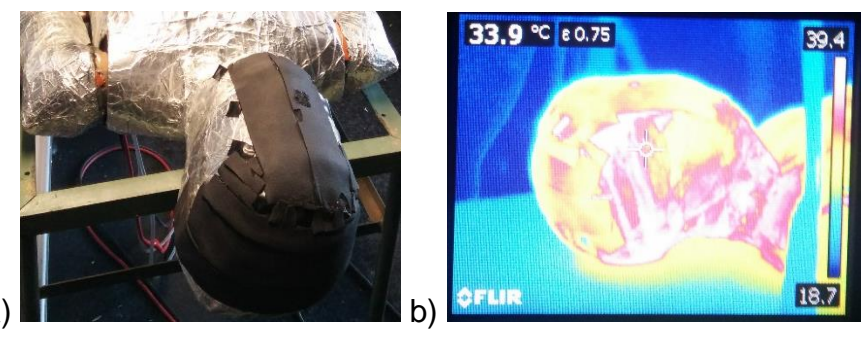


Fig. 28 - Suzy's head: a) with black duct tape; b) temperature measured with a IR camera

The same was done for all objects in the viewing angle of the camera that was supposed to reflect light. We avoided putting tape on the sensors that are placed on the head of Suzy in order to not disturb the correct reading of the temperature. Also, for making sure that we will have the surface temperature of the black duct tape close to the temperature of a human subject, we increased the setpoint temperature of Suzy's head to 37°C.

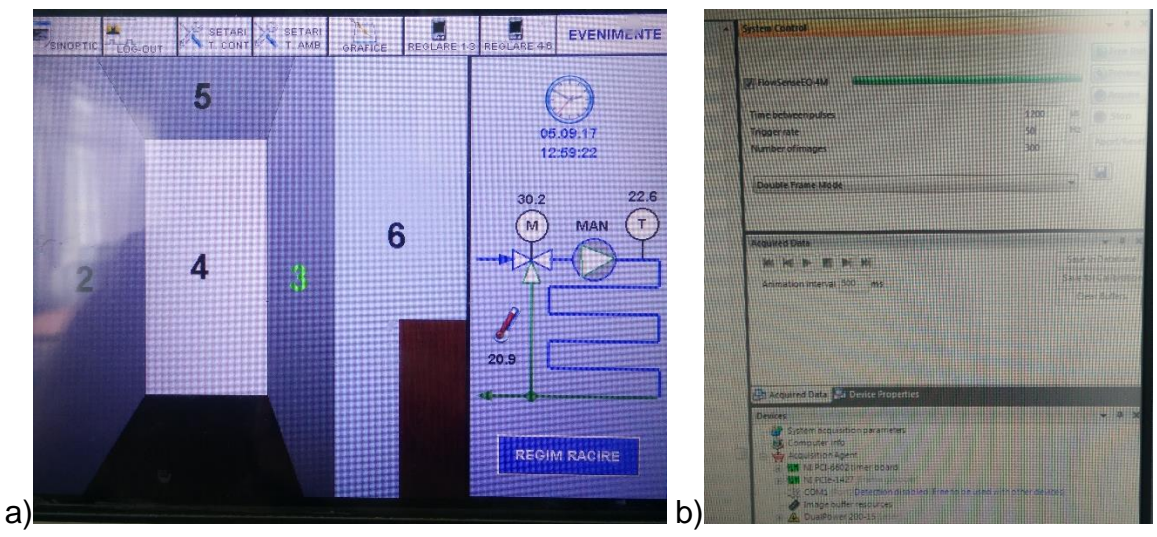


Fig. 29-Suzy's head temperature (with duct tape) measured with a IR camera

We constantly measured the surface temperature with a IR camera to see the temperature evolution on the surface of the duct tape and to make sure that we will not have high temperatures which can cause damage to the manikin (figure 28). The temperature of the walls of the climatic chamber were set to 20°C (figure 29).

The climatic chamber has six (6) individual hydraulic circuit for each wall of the room, including the door. Each circuit has a water recirculation pump, a three-way valve, automatic air release valves and a transducer on the pipe to read temperature. The 6 circuits are connected to a pressure equalizing cylinder that is connected furthered to the heating and cooling generating equipment. On each wall there is a transducer that reads the temperature and sends the analogic signal to the command panel. The wall temperatures can be controlled automatically or manually. Depending on the temperatures read on the walls and on the pipes, depending on the setpoint temperatures and on the PID controller settings, the three-way valve will open or close to a certain percentage and the speed of pumps will be adjusted accordingly. On manually, the percentage will be dictated by the user and the pump will work on manual mode, not automatic.



Fig. 30 – The hydraulic circuits of the climatic chamber

The room can be heated or cooled depending on the needs, on the season. The cooling water is produced by a chiller, with R22 refrigerant, that is placed near the laboratory and the heating water is produced by a boiler placed on a stand in the laboratory (figure 31).



Fig. 31 - The equipment (boiler and chiller) that heats or cools the climatic chamber

The cooling capacity of the chiller is 19.95kW while the heating capacity of the boiler is 24kW. The placement of the measurement equipment with the set-up and the main components can be viewed in the figure 36. The laser was placed on a table, perpendicular to Suzy's head, while the camera was placed in the left side of the laser, rotated at a 90° angle to catch laser plane on Suzy's head. Suzy was placed at ≈1m. The smoke generator was placed on the floor in the right side of the laser, between the thermal manikin and the door of the room. The smoke generation was adjusted to have good density of smoke which does not affect, obstruct, the visual field and which allow us to track the displacement of the particles. Also, the time interval between the two lasers was adjusted to the flow of the fluid, meaning to the air velocity generated by the natural convection of Suzy's head. A picture from the PIV measurements can be seen in figure 32.

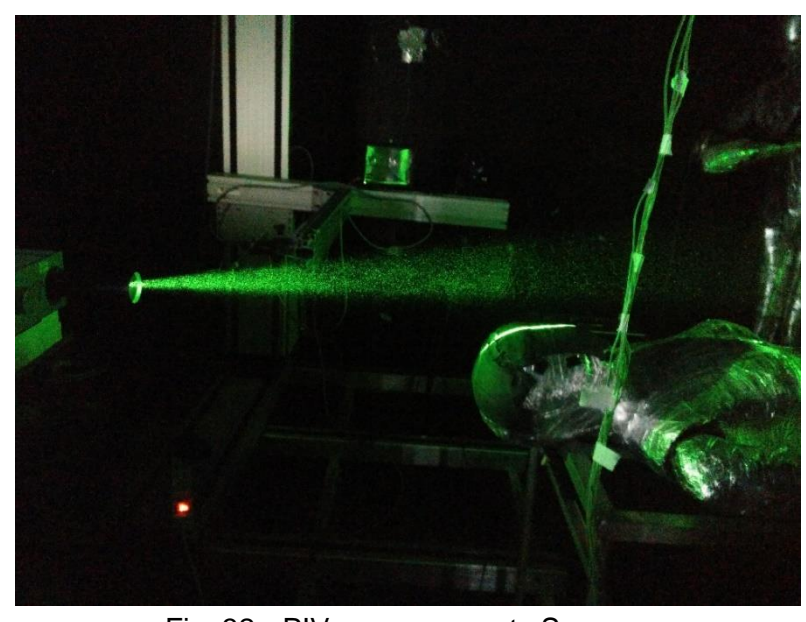


Fig. 32 – PIV measurements Suzy



Fig. 33- PIV measurements Thermal Boy

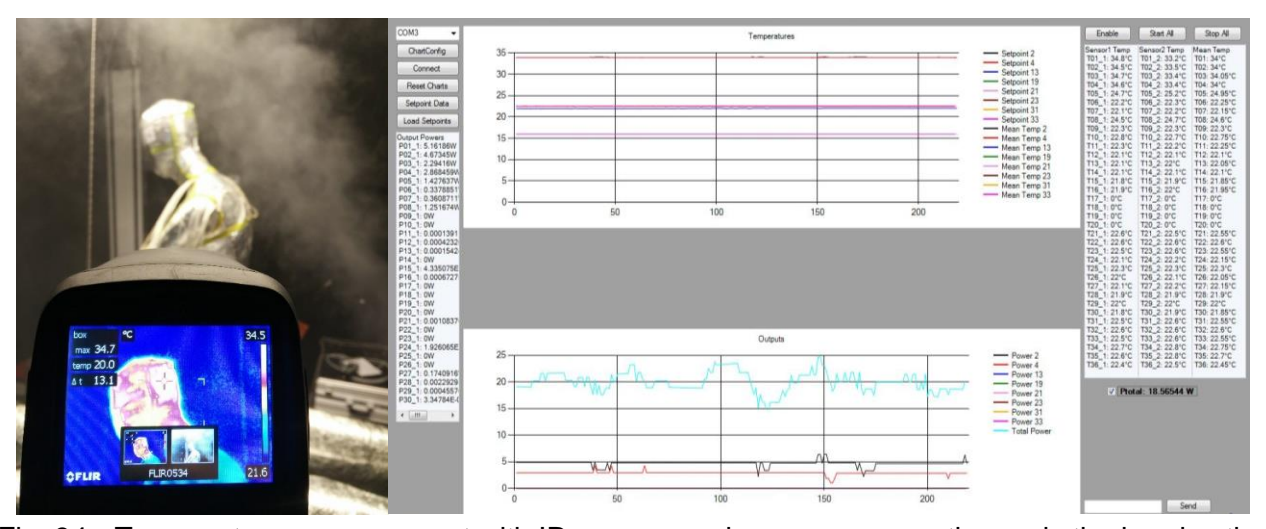


Fig. 34- Temperature measurement with IR camera and power consumption, only the head active

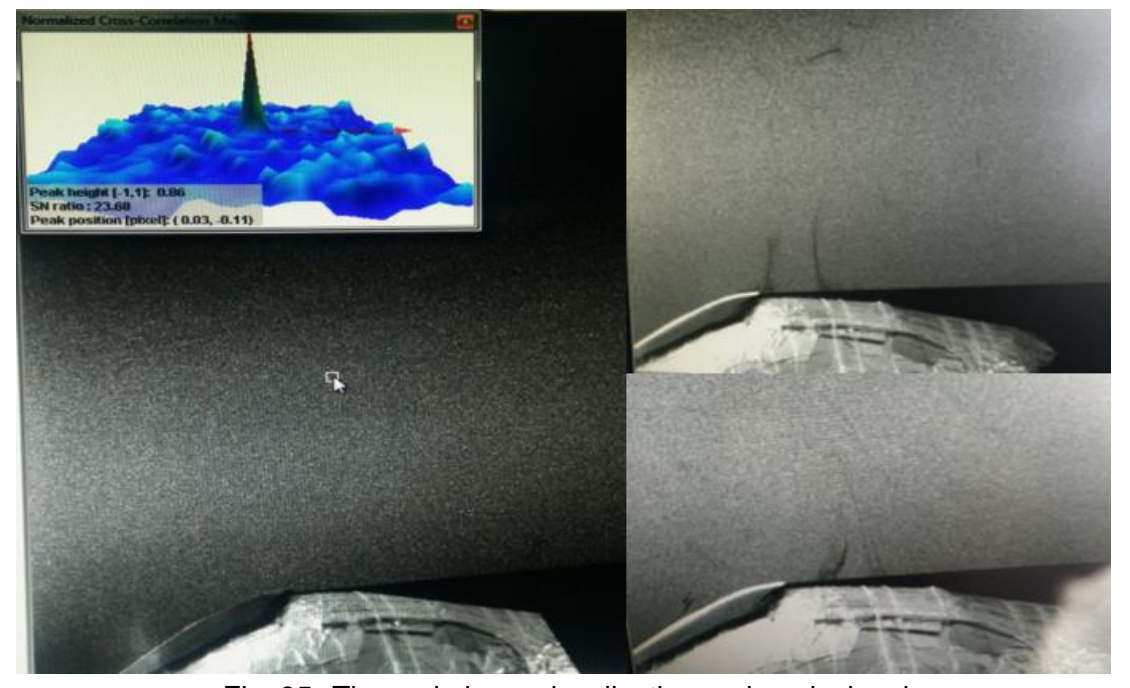


Fig. 35-Thermal plume visualization and peak signal

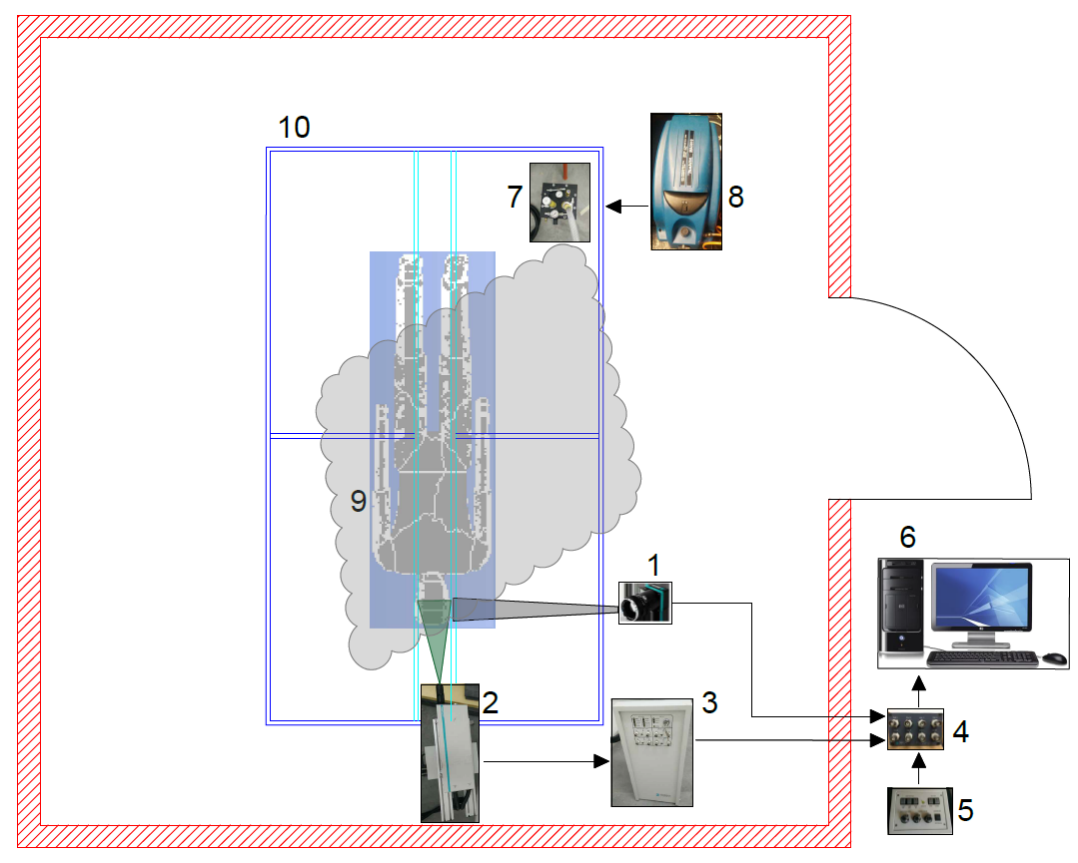


Fig. 36- Equipment placement for the PIV measurements, patient thermal plume

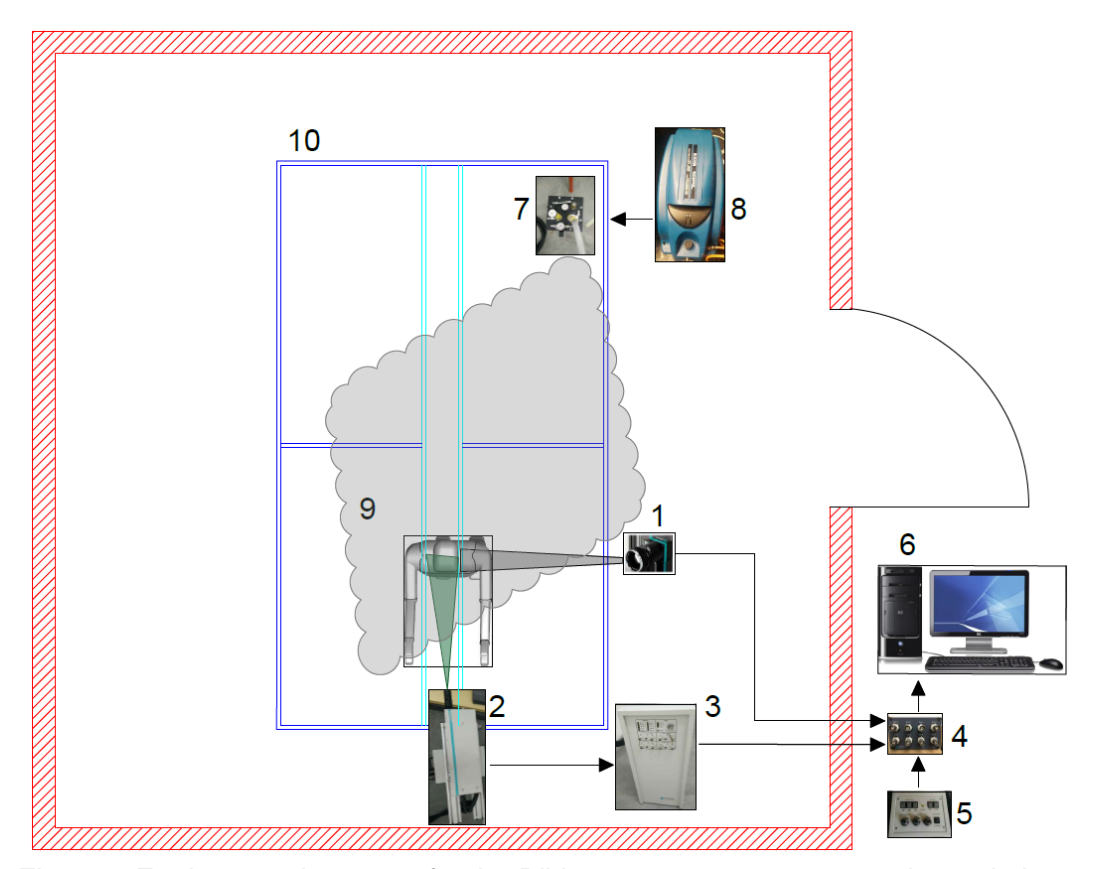


Fig. 37 - Equipment placement for the PIV measurements, surgeon thermal plume

The measurements that regards the passive ways to improve the indoor air quality were made also in the climatic chamber, using the plenum of the air ventilation system of the room to place the eight (8) types of grilles. The different geometries of the grilles can be seen in figure 38. The geometries have been developed in previous studies in which the fluid flow was studied from a single orifice, a single geometry, in experiments involving impact jets or free jets (21, 22).

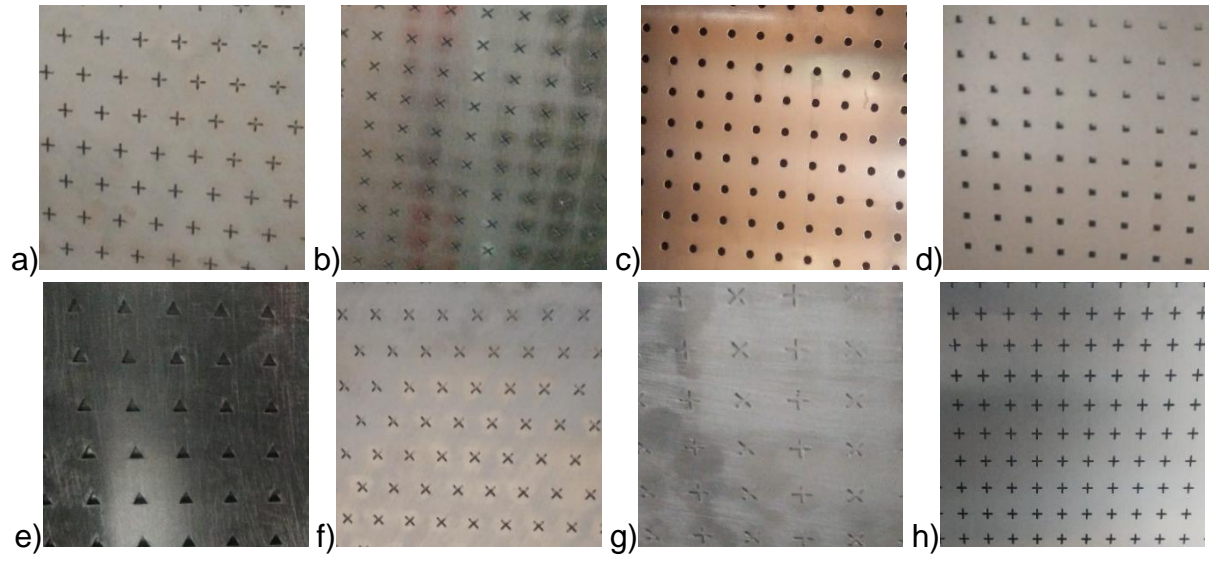


Fig. 38 – The grilles and their geometries

The grilles were numbered with letters for an easier reference (table 1). The dimension of a grille is 1255x635 mm. For covering the whole surface of the plenum, it requires four (4) pieces of a grille. Thus, all eight (8) types of grilles are made in four (4) pieces, resulting in a total of 32 pieces of grilles (8 types x 4 pieces). The plenum has on the middle, on his entire length, a lamp with the width of  $\approx 120$  mm. The plenum is organized on the inside as follows: an enclosure, at the upper part, in which air is supplied, downwards are grilles with round holes, to stabilize the flow, and a place for HEPA filters and at the end the grilles that have different geometries (figure 38).

Table 2 - The grilles numbered with letters

| No. | Grille type      | Fig.25 | Letter |
|-----|------------------|--------|--------|
| 1   | "+" intercalated | a)     | Α      |
| 2   | "x" in line      | b)     | В      |
| 3   | "O"              | c)     | С      |
| 4   | "□"              | d)     | D      |
| 5   | "Δ"              | e)     | Е      |
| 6   | "x" intercalated | f)     | F      |
| 7   | "+" and "x"      | g)     | G      |
| 8   | "+"              | h)     | Н      |

The ventilation system is made of a unidirectional air flow plenum, as a terminal unit, ducts with linear or special pieces, dampers and an axial fan that is connected to a frequency converter from Danfoss, type VLT HVAC Basic Drive FC101. In order to set the same parameters for the axial fan and to characterize the ventilation system (fan, ducts, dampers, plenum) with each of the eight grilles, we made seven (7) frequencies as base points for the measurements. The frequencies were selected to have a minimum air flow which can allow us to make measurements in the range of errors, specified by the manufacturer, of the measuring equipment used and a decent number of measurements between the minimum and the maximum flow of the fan. For each frequency we measured the flow, the pressure loss on the grille, the noise at a height of 1.8 m and 1 m, while we noted the power of the fan and the current injected.



Fig. 39 – The VLT HVAC Basic Drive at 19.0Hz

For measuring the air flow, we used a balometer from TSI, type EBT720/EBT721, with a hood of 610x610 mm made of textile. The hood has almost the same width of a grille and only a half of its length. In the laboratory we have two types of such balometers. For understanding if there are any perturbations or errors in the measuring of the air flow we determine the flow with one balometer, noted the value, then connecting the second balometer to see if disturbances occur at the first one. We expected to see differences of the flow value from the first balometer but we did not see any difference, the value of the flow was still in the range of errors specified by the manufactured. The same result was regardless the position of the balometers on the plenum. Also, through this test we were able to see the if we have the same flow on each grille or the flow changes due to the structure of the plenum, the ducts or the dampers. We saw that with very good approximation the flow was the same on each grille.

For measuring the pressure loss on each grille, we used a differential pressure manometer from Testo, type 521 to which we connected two hoses.

The sound measurements were made with a portable sound meter from Bruel & Kajer, type 2250-S. The sound measurements were made at a medical staff height, ≈1.8m, and a patient height, ≈1m height. For each height we made measurements in four (4) points,

each point was placed approximately in the middle of each grill, recalling that there are four grilles who covers the plenum. A mean value was calculated, from the measured ones, which was used to characterize acoustically the system with the respective grille mounted, for the two heights (1.8m and 1m). Acoustic measurements were made also without the grilles, to determine if the grilles generate sound or acts like an attenuator.



Fig. 40 – Equipment used for measuring

Of course, in every measurement there are errors due to various factors, but we tried to minimize their influence. An example for this is the sealing made between the grilles and the case of the plenum with a duct tape type sponge. Between the grilles and the case of the plenum there are small spaces on each side, do to manufacturing errors, were the flow can escape.

Without a doubt, there are general factors that causes errors in the measurements and here we can specify the equipment reading errors and the human errors (wrong reading, wrong placement of the equipment, too little time for a measurement and so on). Also, there are specific factors that causes errors that depend on the experiment, on the measurements made. The errors that could have occurred here can be the wrong placement of the hood (not tight, sealed enough), the wrong sealing of the spaces between the grilles and the case of the plenum, reading errors, measuring errors.



Fig. 41 – Suzy and Thermal Boy as a patient and a surgeon in the climatic chamber

The data collected from the measurements was used to characterize the system with each type of grille by pressure loss, noise and air flow. Also, we used the measurements to compare each other to see what system has a better performance.

# 4. Numerical part

The numerical studies use Computation Fluid Dynamics (CFD) to capture the global patterns of the flows that are involved in a OR. Often, both types of studies, numerical and experimental, are used to validate one another and to strengthen the credibility of the results [(4, 23)].

# 4.1. The configuration of the numerical case

The purpose for the numerical part was to develop a realistic CFD model of an OR with patient and medical personnel. The numerical study was made in Ansys software, version 15.0, using the Workbench platform that includes Design Builder, for constructing the geometry, and Fluent, for making fluid flow simulations.

The initial numeric case consists in a patient laying on a bed. The second numerical case consists in two surgeons and one patient that lies down on a table. The bodies of all the occupants have an anatomic shape. The virtual manikin has a height of 1.75 m and a body surface of 1.8 m<sup>2</sup>.

The computational grid of the interest domain (figure 43) for the initial case is composed of 3.6 million of tetrahedral elements with a boundary layer that consists of 8 layers. Grid independency test of the solution was performed on four different meshes: 1.3, 2.5, 3.6 and 4.4 million. We chose the 3.6 million elements mesh because there was insignificant difference between this grid and the 4.4 million. For the sizing of the cells we used proximity and curvature as an advanced size function. The relevance was coarse, smoothing high and curvature normal angle 18°. As a boundary layer function, we used inflation with smooth transition option that had transition ration 0.272, 8 maximum layers and a growth rate of 1.2. A face sizing option was applied for the manikin with the table and for the inlet and outlets.

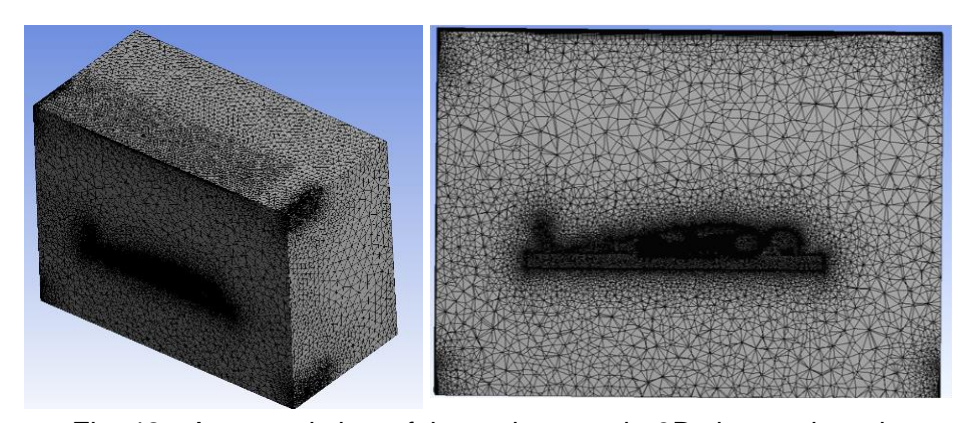


Fig. 42- A general view of the patient mesh, 3D view and section

The element size for the manikin was sated at 10mm with soft behavior, same curvature angle and growth rate, while for the air terminals the sizing was 50mm and the same settings.

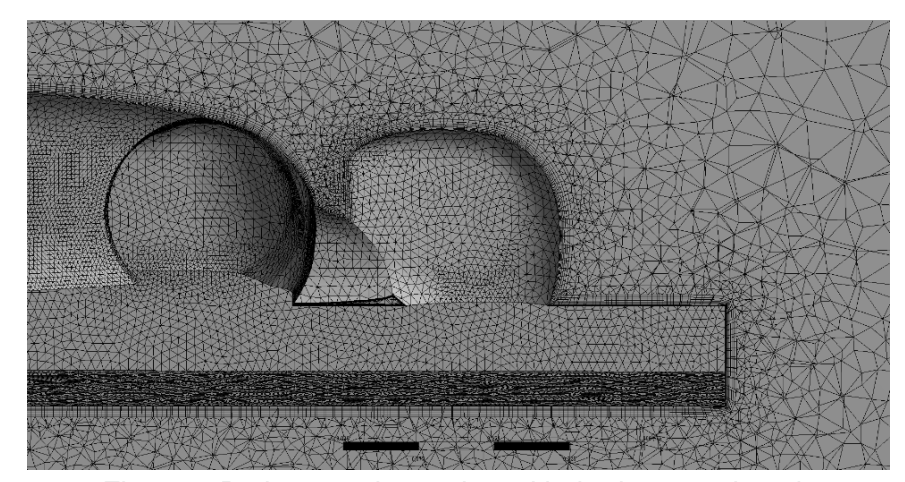


Fig. 43 – Patient mesh, section with the interest domain

The computational grid of the interest domain (figure 46) for the second case is composed of 18.3 million of tetrahedral elements with a boundary layer that consists of 8 layers. A grid independency test of the solution was performed on five different meshes: 10, 11.8, 13.75, 18.3, 20.3 million tetrahedral elements. We chose the 18.3 million elements mesh because there was insignificant difference between this grid and the 20.3 million.

The general mesh sizing was made using curvature and coarse relevance center. The smoothing was done with medium and slow transition, with fine span angle center. Different types of face sizing were made for the outlets, inlet and the manikins.

The boundary layer for the thermal manikins were with first layer high of 0.35 mm and a growth rate of 1.2 because we wanted to calculate the boundary layer. The maximum wall y+ value was 0.91.

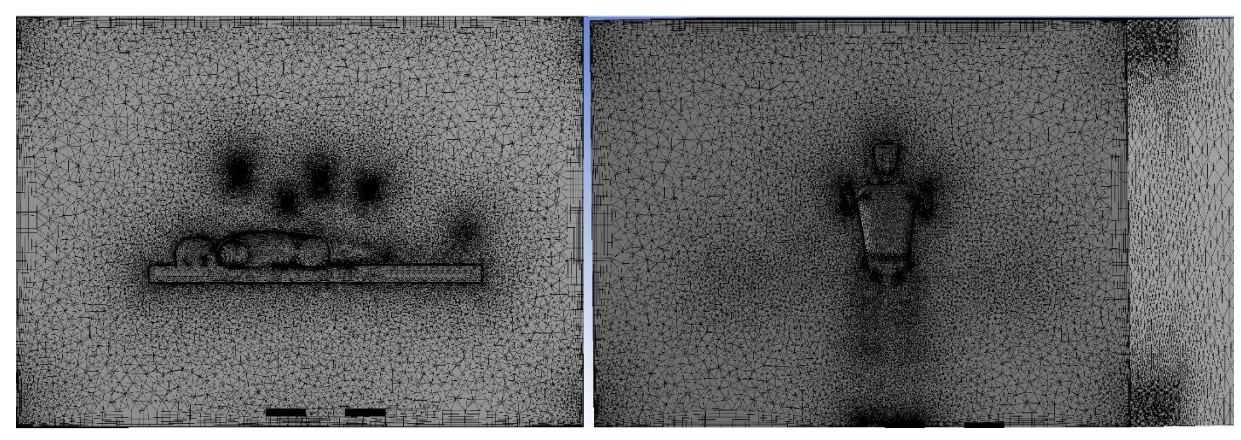


Fig. 44 - Patient and surgeons mesh, a general section view

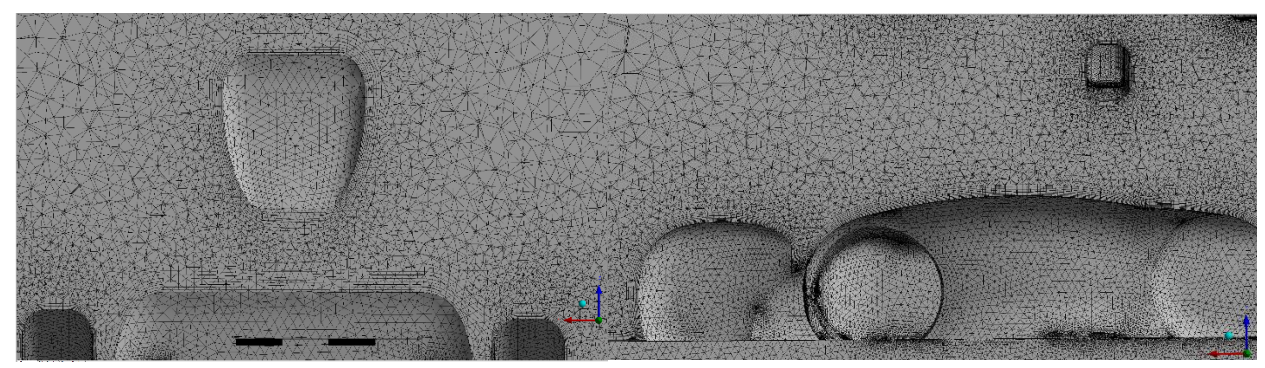


Fig. 45 – Patient and surgeons mesh, section view for the both

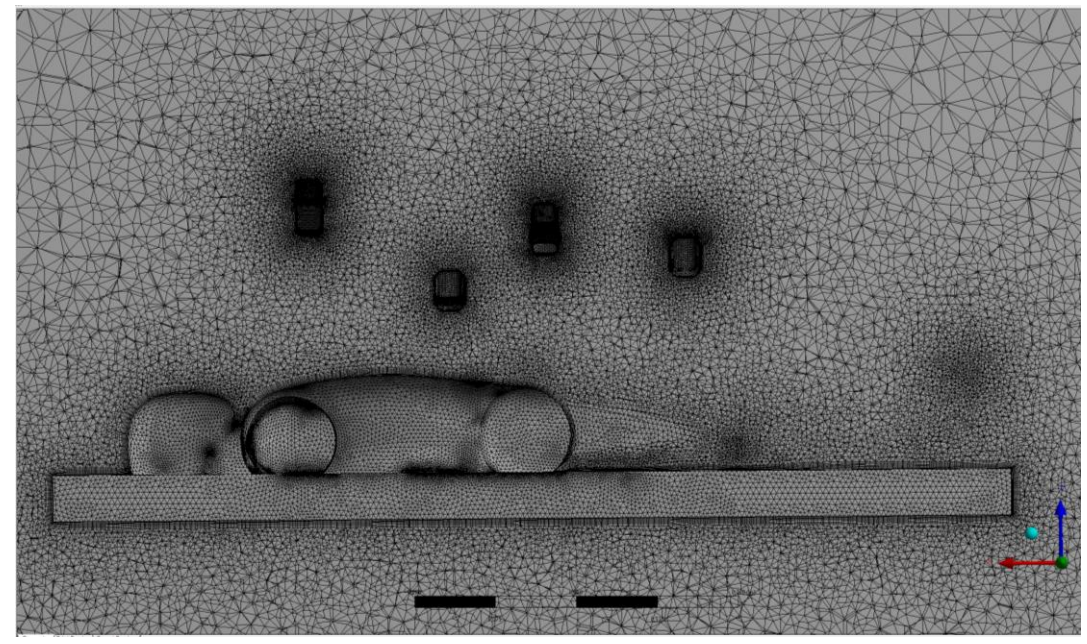


Fig. 46 – Patient and surgeons mesh, section with the interest domain

# 4.2. Equations and parameters used

For the pressure-velocity coupling we utilized the Coupled algorithm. A second order upwind scheme was used to calculate the convective terms in the equations, integrated with the finite volume method. The turbulence model used for the numerical simulation was SST k- $\omega$ , given that the overall performance of this model is one of the best for the indoor environment modelling (3). A low Reynolds and curvature correction was applied, also a production limiter. The governing equations of the flow, equation of mass continuity, transport and energy are:

Mass conservation:

$$\frac{\partial \rho}{\partial t} + \frac{\partial \rho u_i}{\partial x_i} = 0 \tag{10}$$

Momentum conservation:

$$\frac{\partial \rho u_i}{\partial t} + \frac{\partial \rho u_i uj}{\partial x_j} = -\frac{\partial p}{\partial t} + \frac{\partial \left[ \left( \frac{\partial u_i}{\partial x_j} + \frac{\partial uj}{\partial x_i} \right) - \frac{2}{3} \frac{\partial u_i}{\partial x_j} \right]}{\partial x_j} + \rho g_i$$
(11)

Energy conservation:

$$\frac{\partial \rho e}{\partial t} + \frac{\partial \rho u_j e}{\partial x_j} = -\frac{\partial u_j p}{\partial x_j} + \frac{\partial \left(\lambda \frac{\partial T}{\partial x_j} + \mu \left[ \left( \frac{\partial u_i}{\partial x_j} + \frac{\partial u_j}{\partial x_i} \right) - \frac{2}{3} \frac{\partial u_i}{\partial x_j} \right] u_j \right)}{\partial x_j} + S$$
(12)

The boundary conditions used were 24°C walls temperature, different temperatures on the segments of the manikins (table 3) and air velocities from 0.1 to 0.4 m/s, with an increase of 0.1 m/s each time.

Table 3 - Segments temperature

| Head        | 34 °C |
|-------------|-------|
| Core        | 32 ℃  |
| Arms (both) | 30 °C |
| Legs (both) | 27 °C |

#### 5. Results

The objective of the PIV measurements where to validate the thermal plume of the patient and the surgeon from the numerical case. The results of the thermal plume from the PIV measurements and the CFD study are shown below, as a comparation.

The objective of making different geometries for grilles was to determine if with passive solutions we can improve the air distribution and the thermal comfort of the occupants. For this objective, the first step was to make a technical characterization of the grilles by measuring the pressure loss, air flow and noise for each. After this technical characterization, a comparations between is needed to see which one is more performant. A graphic for each system (ventilation system with different type of grille) was made that includes the noise, at a height of 1.8m and 1m, and pressure loss according to the flow (figure 47, 48). Also, comparations between noise levels were made, for each system, to see what acoustic differences can be according to height (figure 49). Another type of comparation made was to see what system performs better in terms of pressure loss and noise level (figure 50, 51, 52).

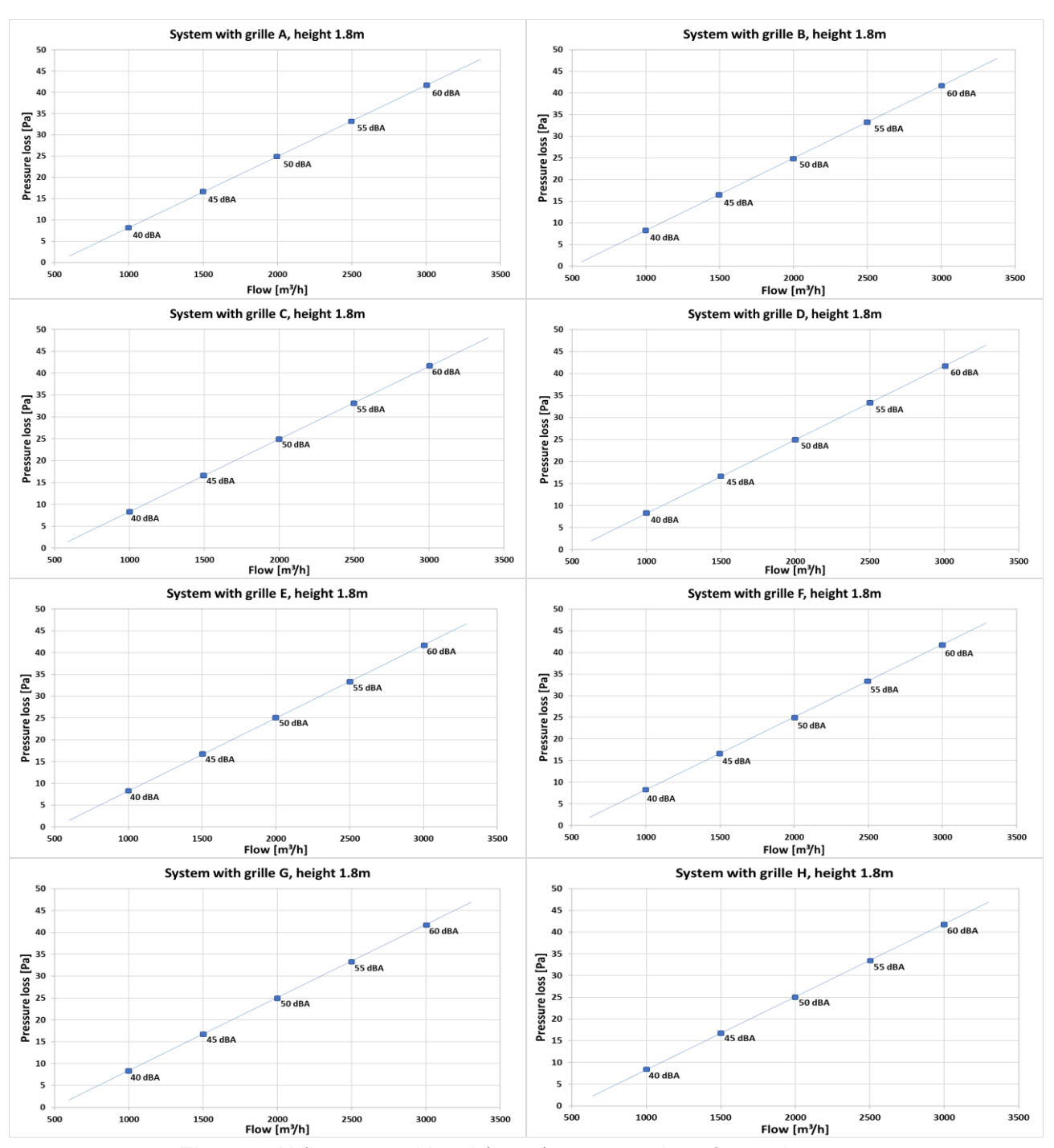


Fig. 47 - Airflow, sound level (1.8m), pressure loss for each system

The technical characterization of each system, with different grille, shown in figure 47 and 48, is in the format of a typical grille graphic that contains air flow, pressure loss, noise level. The high values of noise level are because there was no sound attenuation made and it contains the noise produces by the system as a unit (fan, ducts and other pieces).

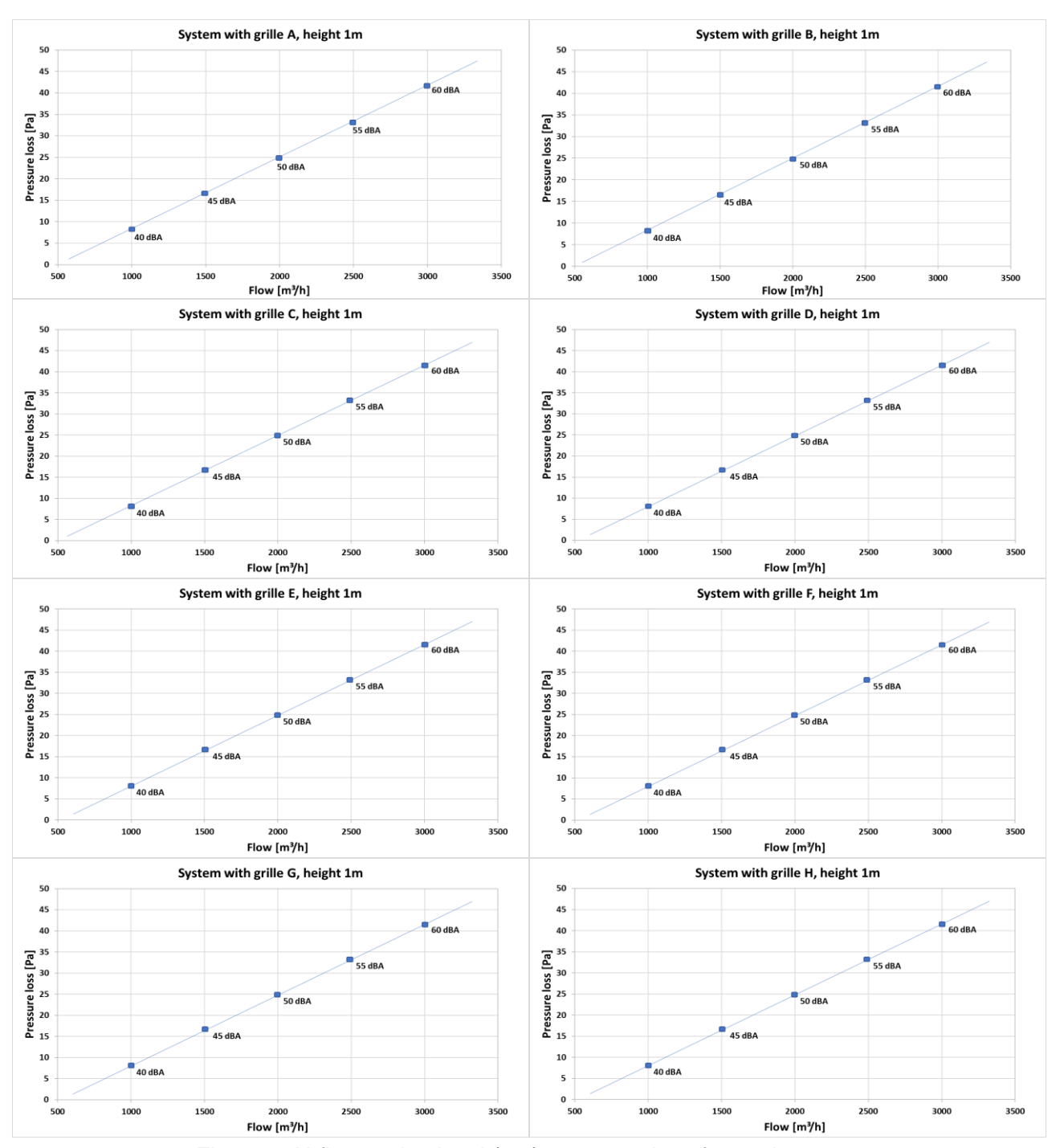


Fig. 48 – Airflow, noise level (1m), pressure loss for each system

Related to the noise level comparations between the two heights, 1.8 and 1m, shown in figure 49 we see very slight differences between the values obtained. The average difference is 1-2 dB, with some peaks in the left part of the graphics, at small flows. This is because at small flows the noise generated by the systems is low and noise perturbations from the exterior can easy influence the measurements. Thus, the peaks are probable due to noise perturbations occurred at the time of measurements.

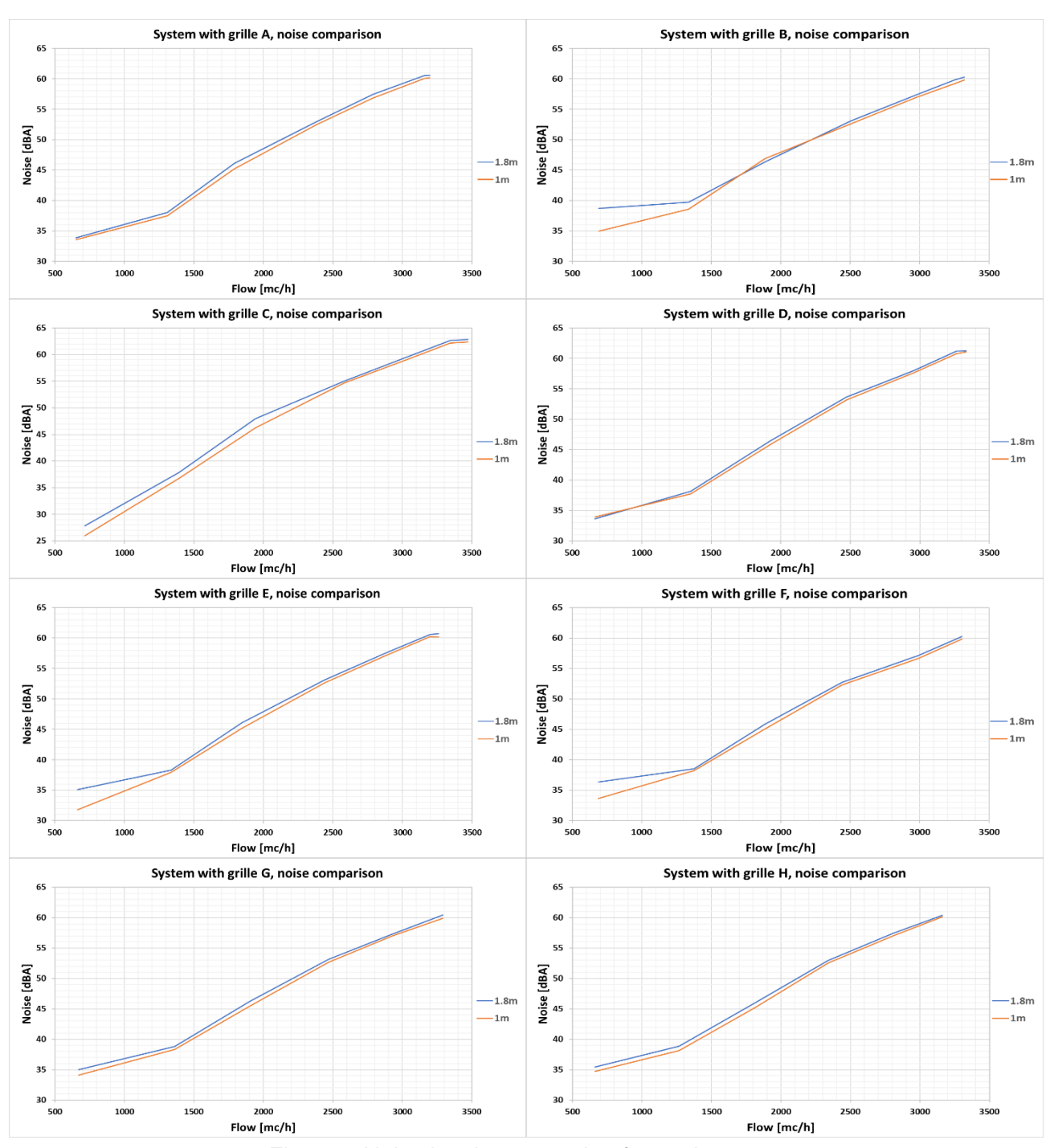


Fig. 49 - Noise level comparation for each system

A comparation of pressure loss, between the systems, is shown in figure 50. The comparation contains the values obtained with the 8 types of grilles. A first observation is that almost all the systems perform slightly the same, with small differences between them, and the only system with E type grille distinguish from the others with a high-pressure loss at high flows. Nonetheless, the difference between system with grille type E and the second one as value, system with grille type A, is not that much, approximately 4 Pa.

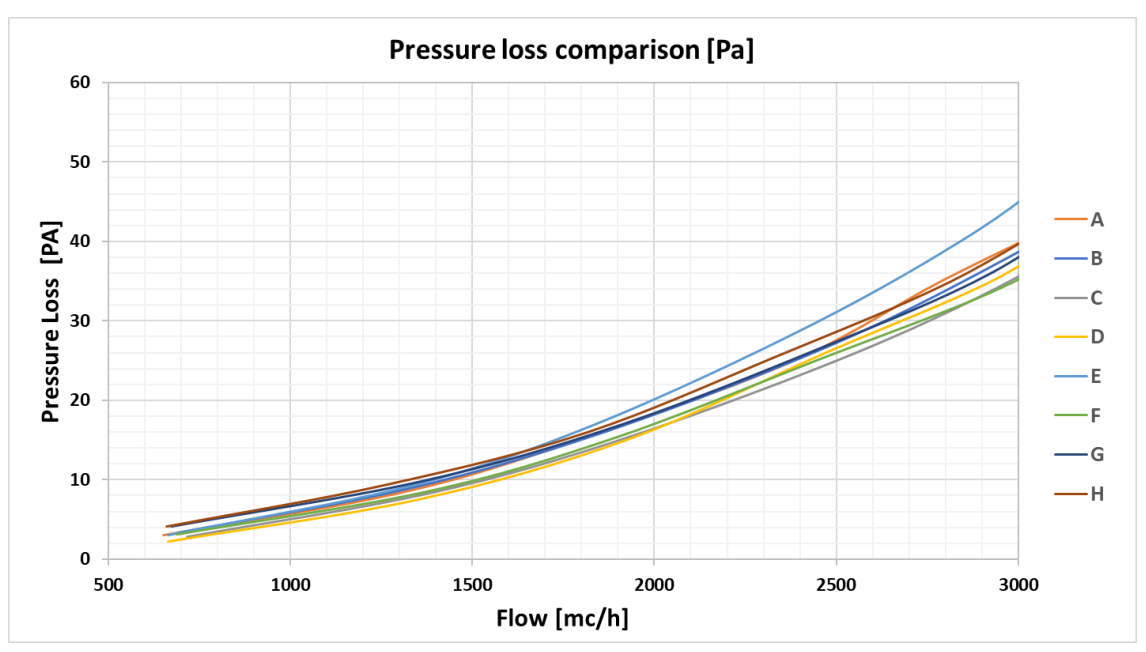


Fig. 50 – Pressure loss comparation between the systems

The comparation of noise level between the systems with the 8 types of grilles and without grilles is shown in figure 51 and 52 for both heights. A first observation is that without grilles the noise level is higher, and this leads to the conclusion that the noise level is attenuated by the grille, regardless of its type. A second observation is that at low flows the measured values have been perturbated in some cases due to external factors. This is because the measurements were made in a normal chamber (the climatic chamber), with no special acoustic protection, as well as o daytime, not just at night, periods where it was possible to have activity in the laboratory or outside that can generate noise.

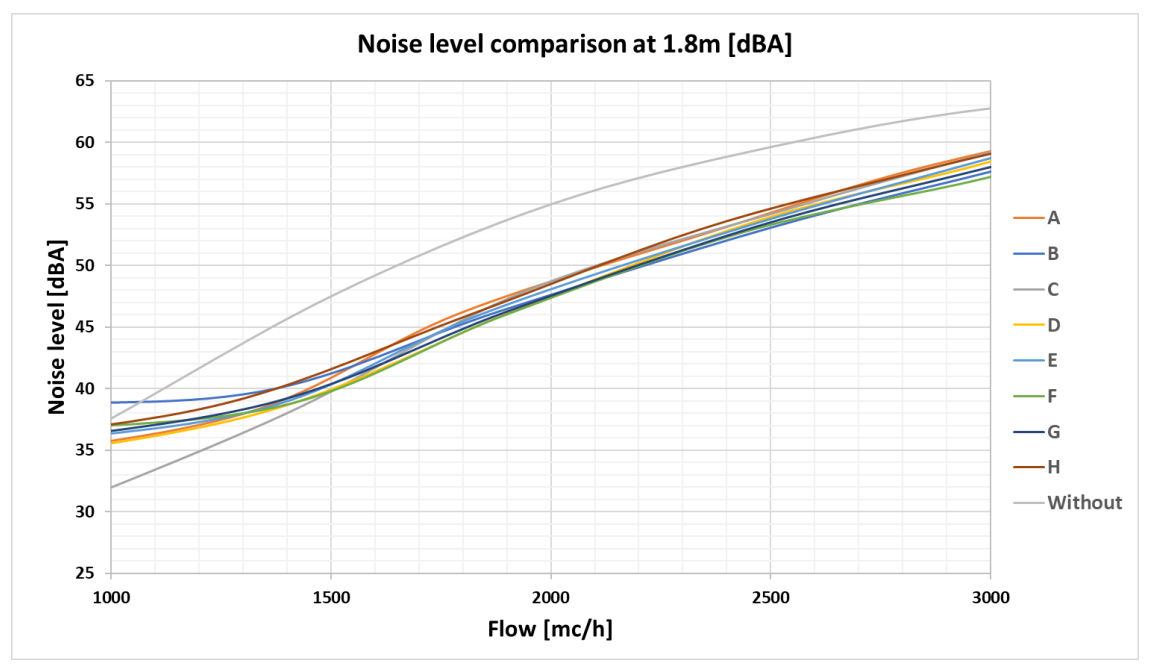


Fig. 51 – Noise level comparation between the systems

A third observation is that the values, regardless of the system, are almost the same with a very slight difference between them. The highest difference being 3 dBA. These three conclusions can be seen to the measurements for both heights.

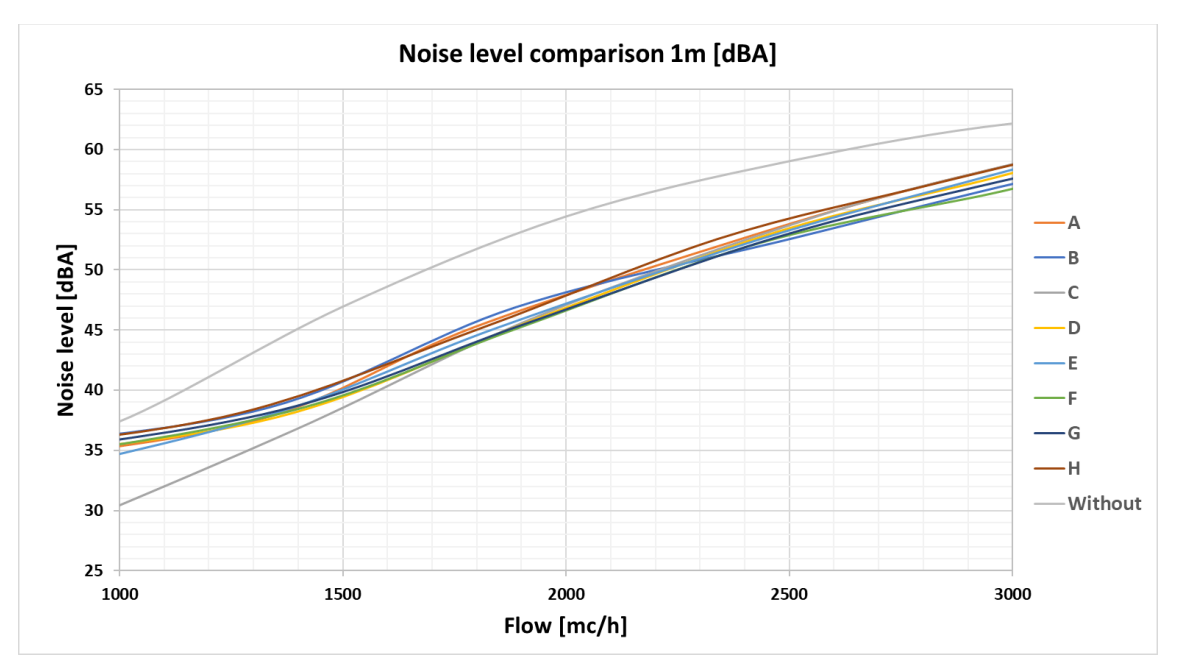


Fig. 52 – Noise level comparation between the systems

The thermal plume of the surgeon analyzed by numeric study is shown in figure 53 and 54. In the first figure we can see the velocity range by contour and vectors, while in the second figure we can see the temperature gradient. We measured the plume for the surgeon by means of PIV but the results obtained were unusual, at least at first attempts.

The experiments were made in the climatic chamber, on several days, all at daytime, in a cooler period of the year (transition from autumn to winter). We found out that the speeds obtained by experimental measurements, for the surgeon, were higher than in the numerical case. From the first data obtained we repeated the measurements, trying to eliminate the potential errors that we thought. Thus, we recalibrated the laser plane, the CMOS camera with a rod (marvel) of 100x100cm, analyze the data with various post-process methods (average correlation, PIV correlation, cross-correlation).

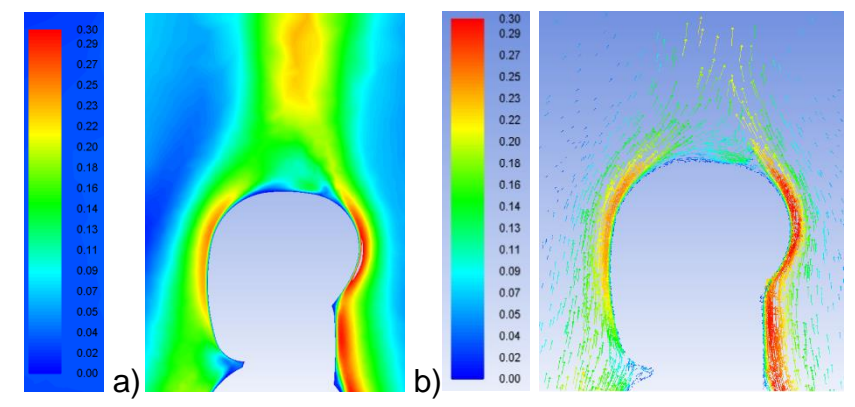


Fig. 53 – Thermal plume velocity of the surgeon: a) contour; b) vectors

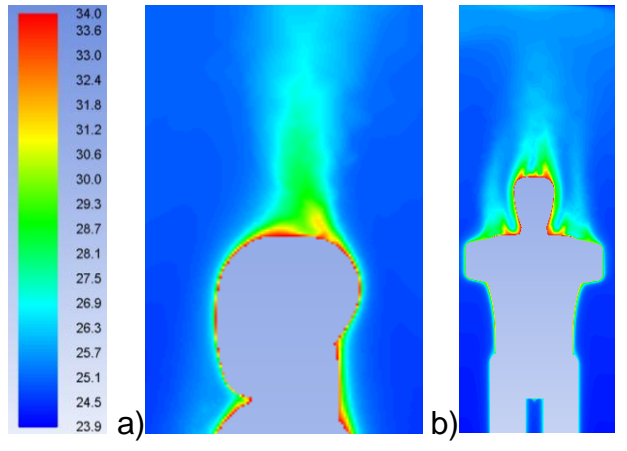


Fig. 54 – Thermal plume gradient temperature of the surgeon

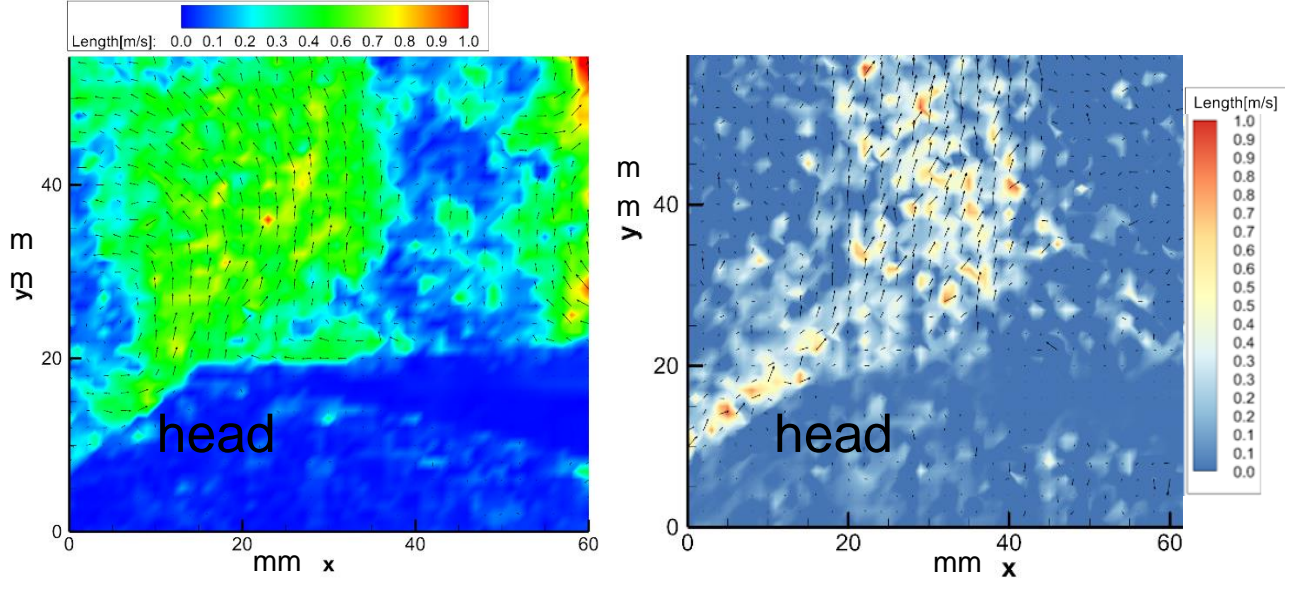


Fig. 55 - Surgeon PIV thermal plume velocity vectors in mm

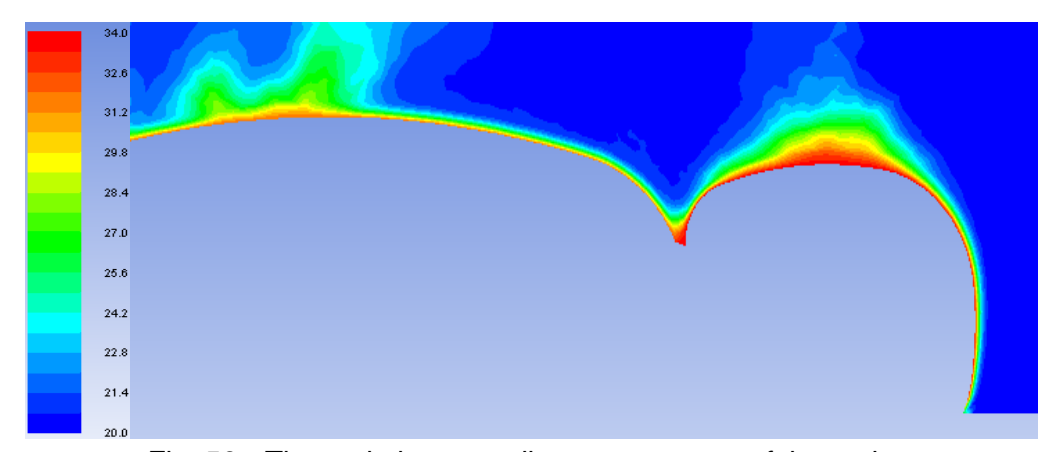


Fig. 56 – Thermal plume gradient temperature of the patient

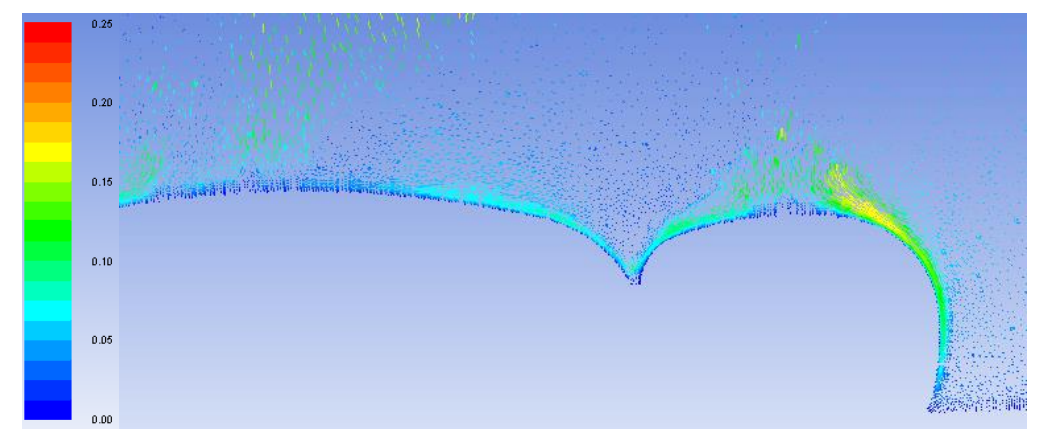


Fig. 57 - CFD thermal plume, velocity vectors of the patient

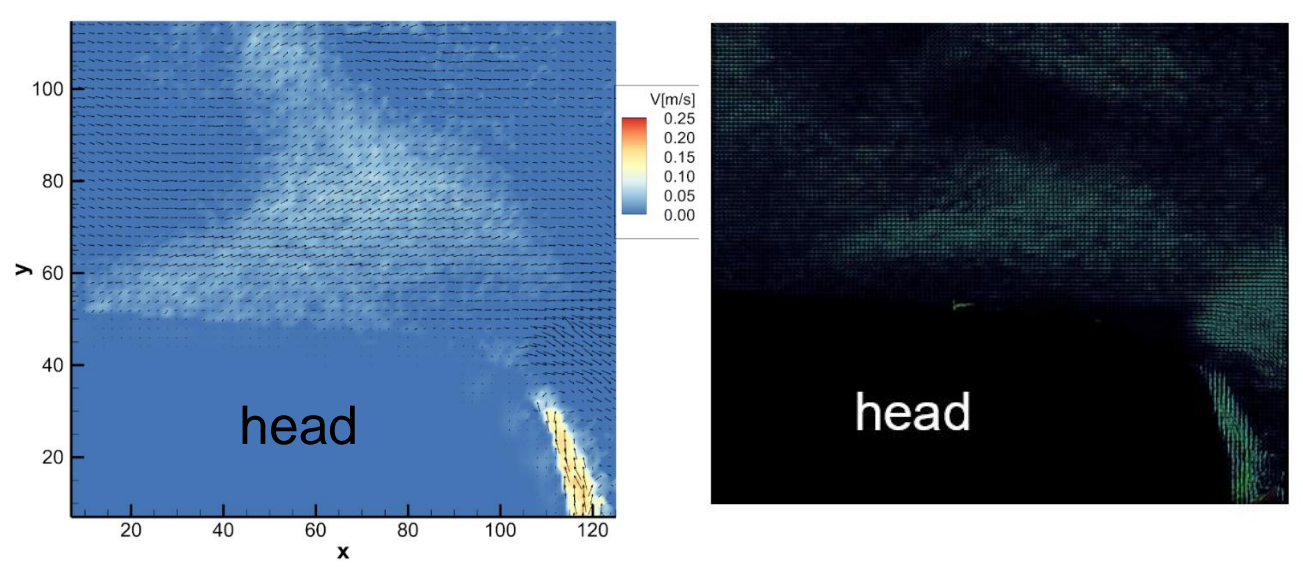


Fig. 58 - Patient PIV thermal plume velocity vectors: left) contours, right) visualization DantecStudio

Other simulations that we run had included the flow around the operating area, surgeons and patient, at different velocities. The different velocities are in the range of the ones recommended by standards, from 0.1m/s to 0.4m/s with a gradual increase of 0.1m/s, and the study area covered only the area with the biggest importance in the room, the operating table. These simulations are presented in figures 61÷64 from a section view in the middle of the patient. The pictures contain the 4 simulations made with the 4 velocity values but with two different scales, one with 0÷0.8 m/s and the other one with 0÷0.5 m/s. The properties selected for showing the vector velocities can be seen in figure 60.

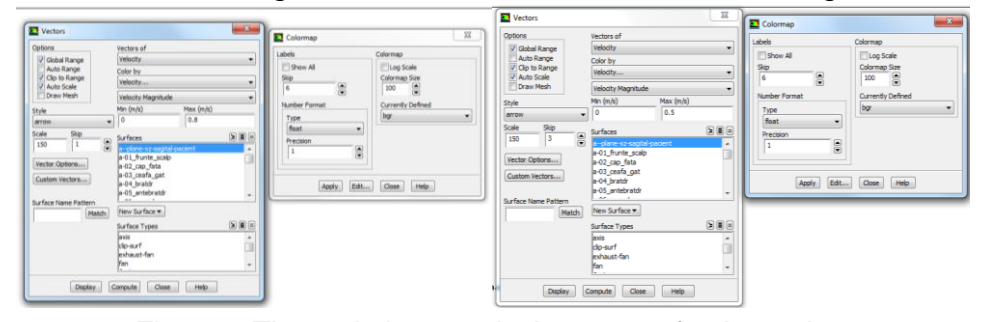


Fig. 59 - Thermal plume, velocity vectors for the patient

In the first two figures (61 and 62) its presented a general section view of the whole numerical case where we can see in section the patient and the hands of the surgeons and the fluid flow from the air terminal towards the operating table. In the second two figures (63 and 64) we paid a close attention to the air movement around the operating table, having the obstruction from the surgeon's hands.

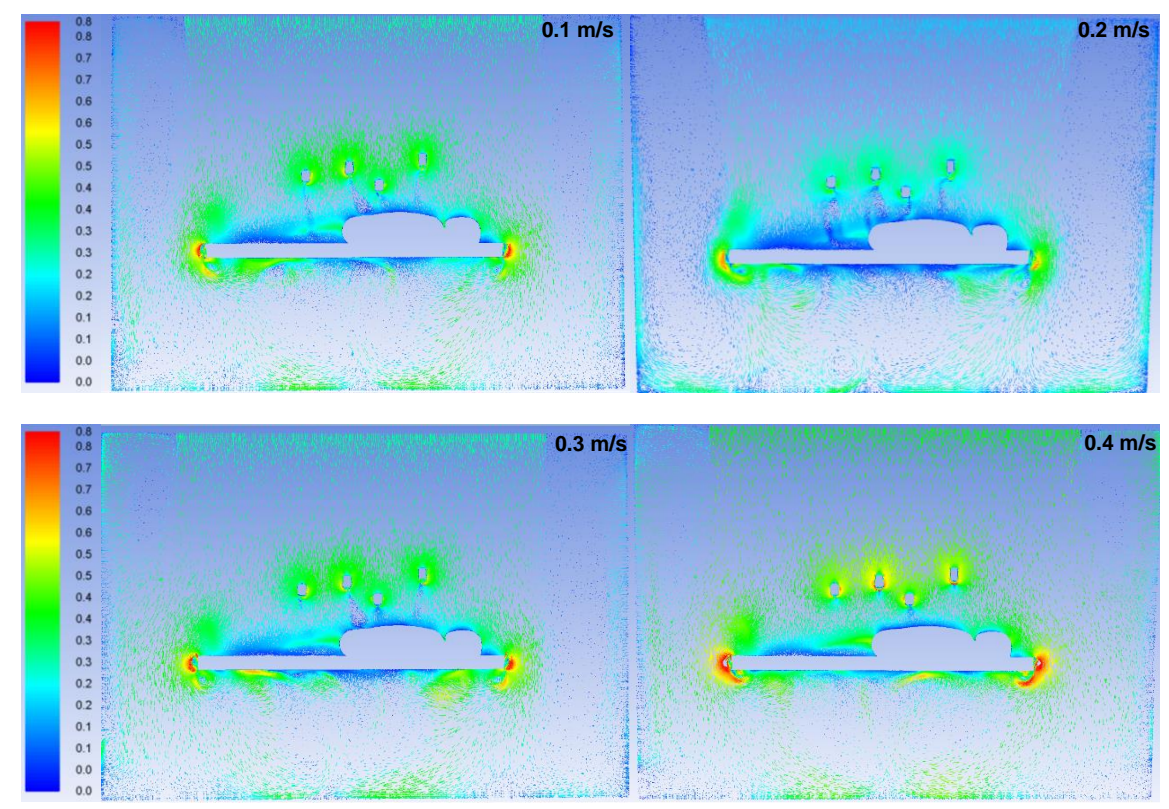
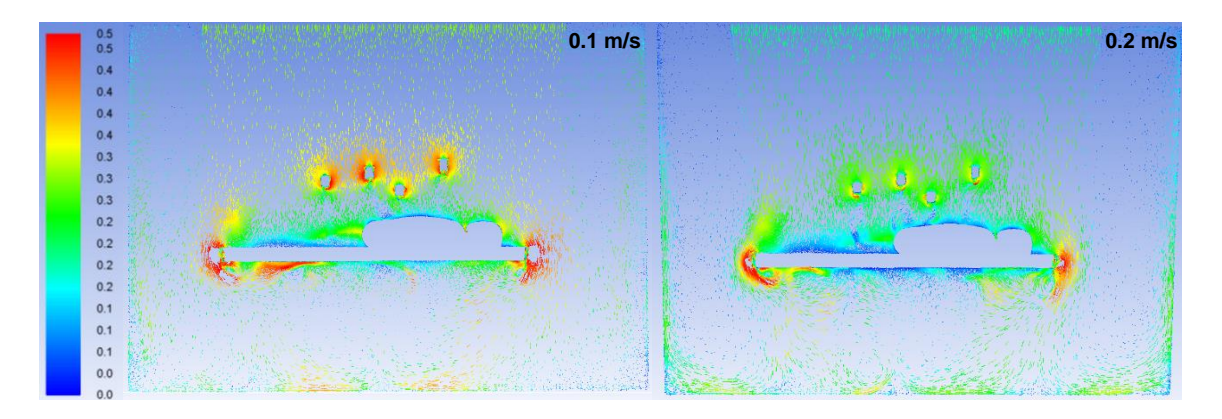


Fig. 60–Thermal plume: general view section, velocity vectors of the patient (0.8 m/s)



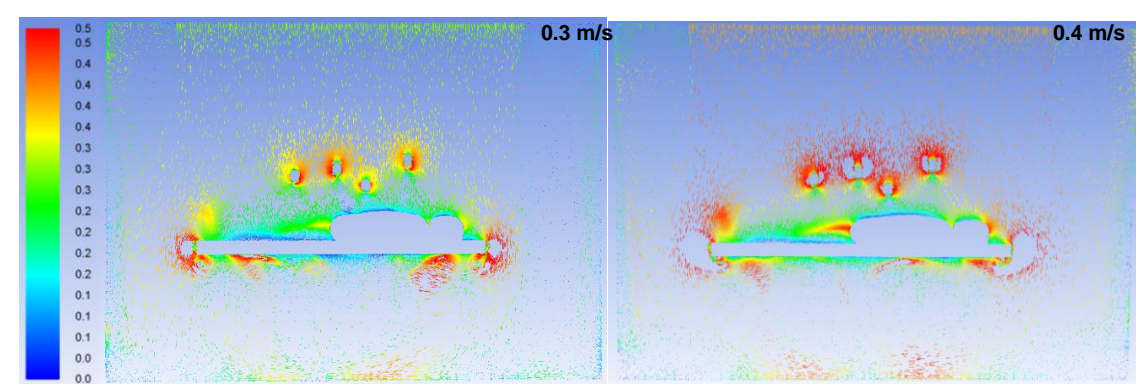


Fig. 61 – Thermal plume: general view section, velocity vectors of the patient (0.5 m/s)

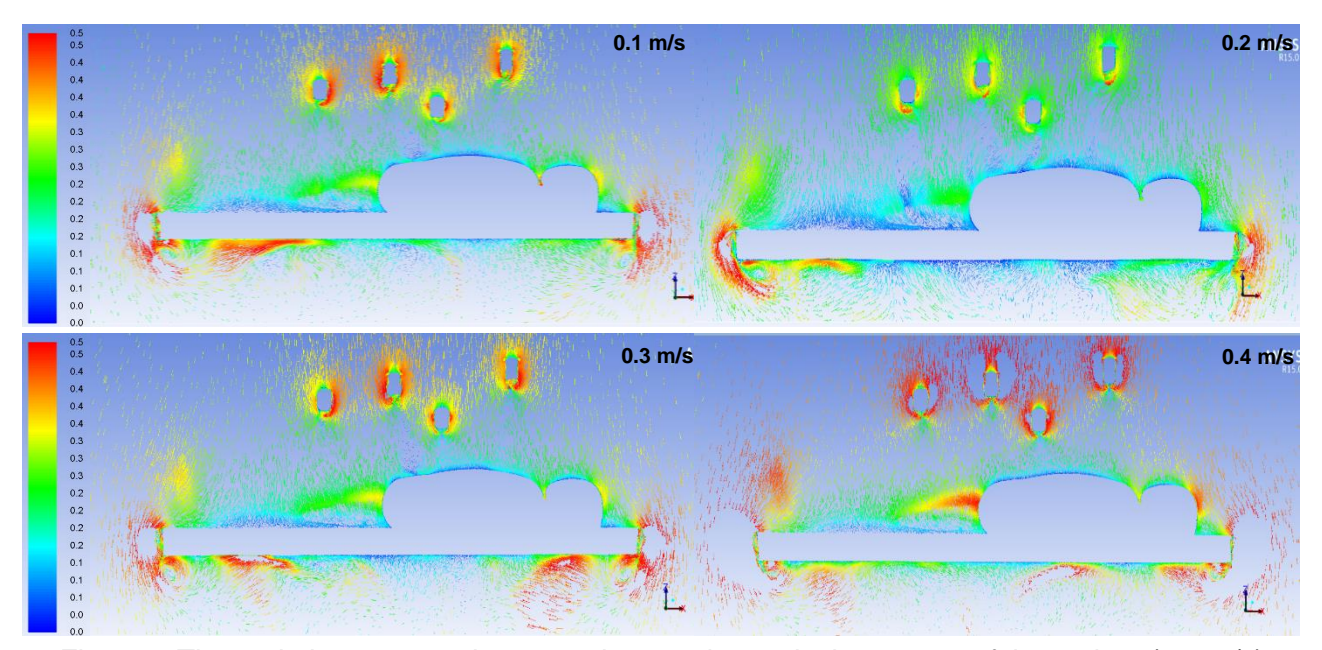


Fig. 62- Thermal plume: operating area view section, velocity vectors of the patient (0.8 m/s)

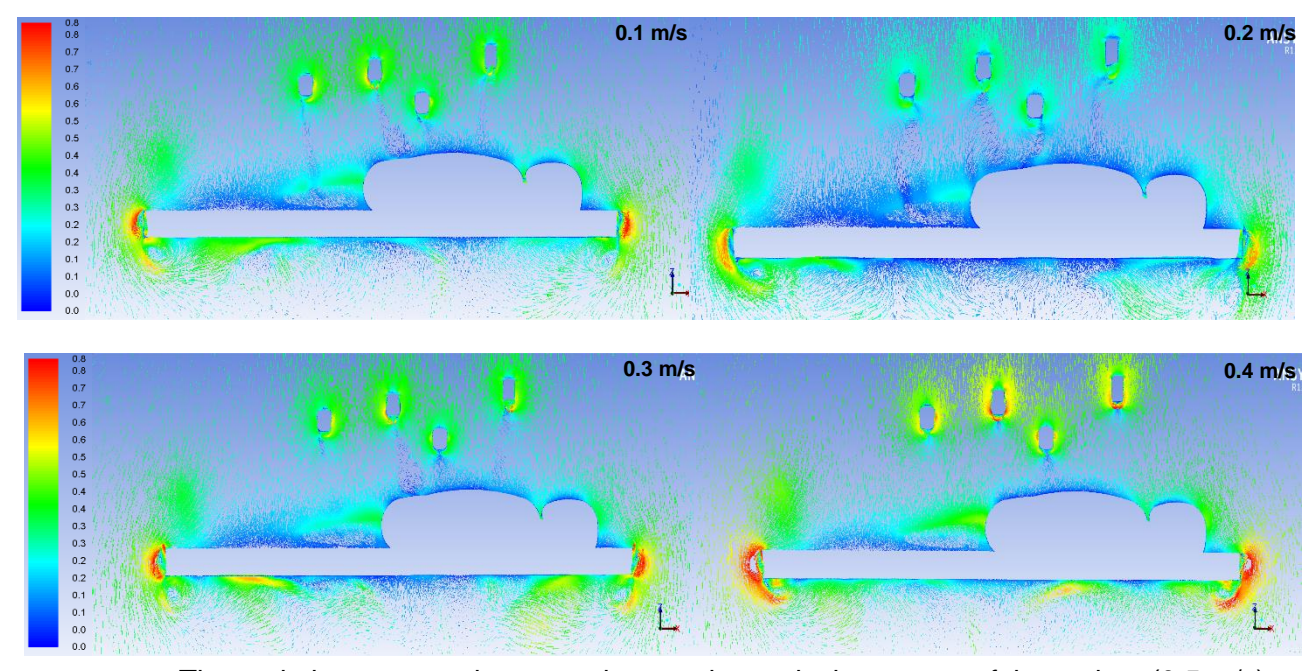


Fig. 63 – Thermal plume: operating area view section, velocity vectors of the patient (0.5 m/s)

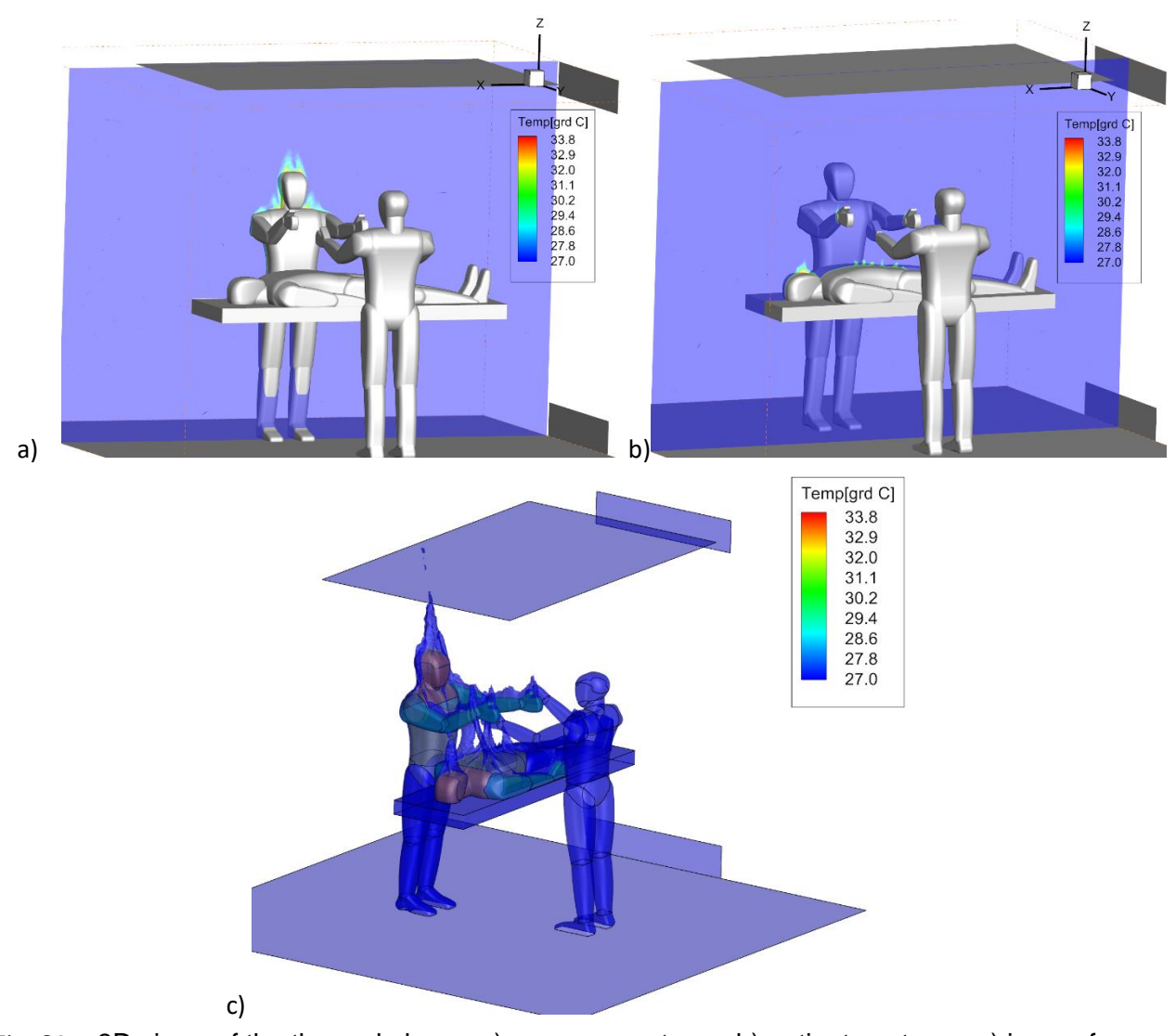


Fig. 64 - 3D views of the thermal plume: a) surgeon contours, b) patient contours, c) iso-surfaces

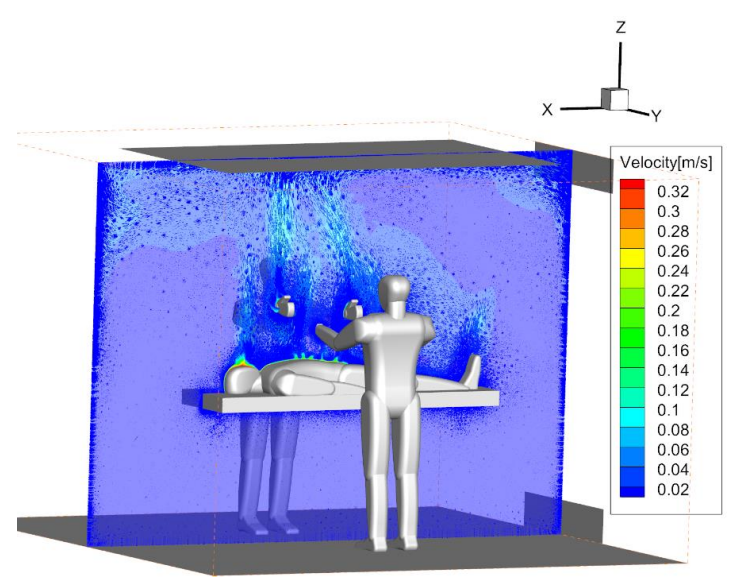


Fig. 65 - 3D views of the thermal plume: slice plane, velocity vectors

## 6. Discussions and future studies

There are a lot of parameters that can be studied in ORs and this is due to their complexity. The numerous examples of situations and parameters that can be studied are observed very well in the literature, the limitations are only in terms of techniques (having the right equipment for measuring or having enough computational power for the CFD simulations). Of course, future studies will take account of these aspects and they will be in accordance with the actual possibilities and the time needed.

Thus, future studies will include thermal comfort measurements with the all 8 types of grilles, improving the numerical case, PIV measurements for validating the new improved case.

The first measurement that we will make its considering mounting the

The thermal comfort measurements will be for all 8 types of grilles with both thermal manikins positioned as a patient and a surgeon, on the same frequencies established from the first set of measurements, measuring the instant temperature on the surfaces of the manikins, calculating the equivalent temperature and the PMV index. The results will be compared in order to see if there are differences, if the differences are big or not and if a geometry has better performance. The better performance in thermal comfort will mean a better air distribution in the room. Also, thermocouples will be mounted on each wall of the climatic chamber and on vertical axis, near the two thermal manikins, allowing us to read the air temperature and the walls temperature.

Improving the numerical case will include a bend over position of the surgeons over the patient, simulating a near to reality situation, and we consider the possibility of a solution that will include local ventilation somewhere in the patient's bed area. The literature will be reanalyzed, to see what type of local ventilation had been used and the results after implementing this system. Also, it will be analyzed if the local ventilation can be implemented in the experimental stand and what types of measurements we can make with him in order to validate it with the numerical case. If the system can be implemented for making experimental measurements, another aspect that may be interesting to study is the implementation of the 8 types of grilles in it and seeing the air distribution for each one. A way o validating the numerical case can be by measuring with the PIV system the air movement and velocities in a plane or more between the two surgeons, this way studying the air movement in the operating area. Because we only have two thermal manikins, for making measurements in the same circumstances as the numerical case, another humanoid manikin will be used as a surgeon. This manikin is a normal one, it doesn't have electronical equipment to measure the temperature, but in this way, we can simulate the presents of a surgeon in the air flow.

## **Bibliography**

- 1. Jankowski T, Młynarczyk M. An impact of the efficient functioning of the ventilation and air-conditioning system on thermal comfort of the medical staff in the operating room. Journal of Ecological Engineering. 2016;17(5):114-9.
- 2. Assessment of Thermal Comfort during Surgical Operations: Hearing before the ASHRAE Winter Meeting Program (2001).
- 3. Kuznik F., Rusaouën G., Brau J. Experimental and numerical study of a full scale ventilated enclosure: Comparison of four two equations closure turbulence models. Building and Environment. 2007;42(3):1043-53.
- 4. Fu S, Biwole PH, Mathis C. Numerical and experimental comparison of 3D Particle Tracking Velocimetry (PTV) and Particle Image Velocimetry (PIV) accuracy for indoor airflow study. Building and Environment. 2016;100:40-9.
- 5. Francesco Romano LM, Jan Gusten, Cesare M. Joppolo. Numerical and experimental analysis of airborne particles control in an operating theater. Building and Environment. 2015;89:369-79.
- 6. Winslow CEAH, L P & Gagge, A P. Physiological reactions to environmental temperature. American Journal of Physiology. 1937;120:1-22.
- 7. Gagge AP. The Linearity Criterion as Applied to Partitional Calorimetry. American Journal of Physiology -- Legacy Content. 1936;116(3):656-68.
- 8. Gagge AP, editor Rational temperature indices of man's thermal environment and their use with a 2-node model of his temperature regulation. Federation Proceedings; 1973.
- 9. Adolf Pharo Gagge APF, L.G. Berglund. A standard predictive index of human response to the thermal environment. Atlanta, GA: ASHRAE Transactions; 1986. p. 709-31.
- 10. Dantec Dynamics AS. ComfortSense 2017 [cited 2017 23.02.]. Available from: https://www.dantecdynamics.com/comfortsense.
- 11. ASHRAE ASoHRaACE-. Thermal Environmental Conditions for Human Occupancy. ANSI/ASHRAE Standard 55: ASHRAE; 2004.
- 12. Fanger PO. Calculation of Thermal Comfort: Introduction of a Basic Comfort Equation. ASHRAE Transactions. 1967;73(2):III4.1-III4.20.
- 13. ISO 7730 Ergonomics of the thermal environment Analytical determination and interpretation of thermal comfort using calculation of the PMV and PPD indices and local thermal comfort criteria. 2005.
- 14. Hensen JLM. ON THE THERMAL INTERACTION OF BUILDING STRUCTURE AND HEATING AND VENTILATING SYSTEM: Technical University of Eindhoven; 1991.
- 15. Noel Djongyang RT, Donatien Njomo. Thermal comfort: A review paper. Renewable and Sustainable Energy Reviews. 2010;14:2626–40.
- 16. Fanger PO. Thermal comfort, analysis and application in environmental engineering. In: Press DT, editor.; Copenhagen1970.
- 17. Charles KE. Fanger's Thermal Comfort and Draught Models. Institute for Research in Construction, National Research Council of Canada, 2003.
- 18. ASHRAE ASoHRaACE-. Thermal Environmental Conditions for Human Occupancy. ANSI/ASHRAE Standard 55: ASHRAE; 2004.
- 19. ASHRAE. Thermal Environmental Conditions for Human Occupancy. ASHRAE Standard 55-1992. Atlanta, GA1992.
- 20. A/S DD. Particle Image Velocimetry (PIV) 2017. Available from: https://www.dantecdynamics.com/particle-image-velocimetry.
- 21. Nastase I. Strategii performante pentru creșterea calității ambientale în sălile de operație (EQUATOR). UTCB: 2016.

- 22. Nastase I, Croitoru C, Dan M, Ursu I, Meslema A. Experimental Study for the integration of an Innovative Air Distribution System in Operating Rooms. Sustainable Solutions for Energy and Environment, EENVIRO 2016; 26-28 October 2016; Bucharest, Romania2016.
- 23. Yao T, Lin Z. An experimental and numerical study on the effect of air terminal types on the performance of stratum ventilation. Building and Environment. 2014;82:431-41.